

Self-consistent solutions of Ginzburg–Landau equations and superconducting edge-suppressed states in magnetic field

G.F. Zharkov, V.G. Zharkov and A.Yu. Zvetkov

P.N. Lebedev Physics Institute, Russian Academy of Sciences, Moscow, 117924, Russia

(August 10, 2000)

Self-consistent solutions of the Ginzburg–Landau system of equations, which describe the behavior of the order parameter ψ , and the magnetic field distribution B , in a long superconducting cylinder of finite radius R , in external magnetic field H , when a vortex line, carrying m flux quanta, is situated on the cylinder axis (a giant m -vortex state), are studied by using numerical method. If the field H exceeds some critical value $H_s^{(m)}$, the giant m -vortex state solution becomes unstable (in response to small fluctuations in its shape) and the solution passes to a new stable edge-suppressed form. The quantum number m in this state does not change, but the order parameter diminishes by a jump (almost to zero) near the cylinder surface; however, superconductivity remains in the deep, at some distance from the cylinder axis. This edge-suppressed state exist in the fields $H_s^{(m)} < H < H_c^{(m)}$, where $H_c^{(m)}$ is the field, in which the second order phase transition into the normal state occurs. (In the case of large radii R and finite m the field $H_c^{(m)}$ coincides with the critical field H_{c2} , in which the superconductivity vanishes in the bulk.) If the magnetic quantum number m is large, the edge-suppressed state degenerates into the usual state of surface superconductivity, and may survive up to the field $H_{c3} = 1.69H_{c2}$. The magnetic moment, the total magnetic flux, the Gibbs free energy and other characteristics of the system are found, as functions of the field H and temperature T , for different radii R , quantum numbers m and parameters κ of the Ginzburg–Landau theory. The intervals of R , T , κ , m are found, where the edge-suppressed solutions exist. The giant m -vortex states exist in both type-I and type-II superconductors, but the edge-suppressed solutions are possible only in type-II superconductors (with $\kappa > 1/\sqrt{2}$). The paramagnetic effect in mesoscopic samples and also the possible connection of the theory and experiment are shortly discussed.

I. INTRODUCTION

The behavior of finite size superconductors in magnetic field was studied on the base of nonlinear system of Ginzburg–Landau equations [1] in numerous theoretical papers (see, for instance, [2–15]). The results of [2–15] were used, in particular, to explain some anomalies, observed in a number of experiments with small size superconductors, placed in external magnetic field [16–24].

In our recent paper [25], by using numerical methods, the self-consistent solutions of nonlinear Ginzburg–Landau equations were studied, for a long superconducting cylinder of finite radius in external axial magnetic field, with no vortices inside the cylinder ($m = 0$). It was found, that type-II superconducting cylinder, which is in the Meissner (vortex-free) state, upon increasing the field H , may pass by a jump into a special (also vortex-free) edge-suppressed state. The order parameter ψ in this state is strongly suppressed (practically to zero) in the vicinity of the cylinder surface, however, the superconductivity survives near the specimen center, where ψ remains finite. Such edge-suppressed solutions were not studied previously [1–15].

Apart from the the Meissner-state ($m = 0$) more general one-dimensional solutions exist, when the vortex line, carrying arbitrary number of flux quanta ($m =$

1, 2, 3, ...), is situated on the cylinder axis. Such solutions (which are called "the giant-vortex states") have been extensively studied in the literature ([2–30]) and used in the interpretation of experiments. The shape of the giant-vortex changes smoothly with the external field H . As is shown in the present paper, for a cylinder of finite radius, the giant-vortex state (with vorticity $m > 0$) becomes unstable, when the field H exceeds some critical value $H_s^{(m)}$. After that, the giant-vortex solution transforms its shape by a jump and acquires the "edge-suppressed" form with the same vorticity m . Such edge-suppressed states are characterized by a strongly suppressed value of the order parameter ψ near the cylinder boundary, and are analogous to the edge-suppressed (or, rim-suppressed) states, found in [25] for the case $m = 0$. Previously, such edge-suppressed modifications of the giant-vortex states were not studied in detail, though some evidence of the edge-suppression was noticed also in [2,3,7].

We should stress, that the edge-suppressed state is noting else, but the usual giant m -vortex solution in a field $H > H_s^{(m)}$. If the field H is increased further, the edge-suppressed solution continues to vary its form, the maximal value of the order parameter $\psi_{max}^{(m)}$ gradually diminishes, and for $\psi_{max}^{(m)} \ll 1$ the edge-suppressed solution may be expressed in terms of the Kummer functions (see,

for instance, [6,8]).

As is shown below, the edge-suppressed states can be formed only in type-II superconductors, with $\varkappa > 1/\sqrt{2}$, where \varkappa is the Ginzburg-Landau parameter. In type-I superconducting cylinder, with $\varkappa < 1/\sqrt{2}$, the edge-suppressed states do not exist.

It is known, that for $m > 0$ the order parameter vanishes in the vicinity of the cylinder axis according to the law $\psi(r) \sim r^m$ [29]; if the field increases, ψ vanishes also near the surface (where the edge-suppressed state forms), so, the superconductivity persists only at some distance from the cylinder axis. If the magnetic quantum number m is increased, the region, where the order parameter $\psi(r) \neq 0$, shifts more and more toward the cylinder surface. For a fixed cylinder radius ($R = \text{const}$, $\varkappa > 1/\sqrt{2}$) there exists some maximal value $m = m_{max}$, for which the edge-suppressed state degenerates into the usual state of the surface superconductivity [26–30].

The transition of a superconducting cylinder into the edge-suppressed state may be accompanied by jumps in the dependencies versus H of such quantities, as: the specimen magnetic moment ($-4\pi M$); the total magnetic flux, captured inside the system (Φ_1); the system Gibbs free energy (G); and by peculiarities in the behavior of other parameters, which characterize the superconducting state. These topics are discussed below in detail. No immediate comparison of the theory with the experiment is possible, because the model case of an infinitely long cylinder approximates the real samples geometry [16-24] very remotely. However, a number of qualitative predictions, which follow from this model, may be used for interpreting some of the peculiarities, observed in the experiments with mesoscopic samples. In particular, the controversial paramagnetic Meissner effect in superconductors is shortly discussed below, basing on the Ginzburg-Landau theory approach.

The paper is organized as follows. In Sec. 2, the basic equations and the boundary conditions of the problem are written. The numeric algorithm, used to find the self-consistent solutions of nonlinear system of equations, is shortly described. Sec. 3 contains the results of numerical calculations. We are forced to present our results by a large number of graphics, which illustrate different details of the system behavior in this many parameter problem (the solutions depend on m , \varkappa , R , H , the specimen temperature T , the critical temperature T_c and the coherence length ξ_0). The necessary comments accompany the presentation of the material. Sec. 4 contains a short resume and discussion of the results.

II. THE SETTING OF THE PROBLEM

Consider long superconducting cylinder of radius R in the external magnetic field H , which is parallel to the

cylinder element. The basic system of the Ginzburg-Landau equations [1] is of the form

$$\text{rot rot } \mathbf{A} = \frac{4\pi}{c} \mathbf{j}_s, \quad \frac{4\pi}{c} \mathbf{j}_s = \frac{\psi^2}{\lambda^2} \left(\frac{\phi_0}{2\pi} \nabla \Theta - \mathbf{A} \right),$$

$$\nabla^2 \psi - \left(\nabla \Theta - \frac{2\pi}{\phi_0} \mathbf{A} \right)^2 \psi + \frac{1}{\xi^2} (\psi - \psi^3) = 0,$$

where \mathbf{A} is the vector-potential of the magnetic field ($\mathbf{B} = \text{rot } \mathbf{A}$), \mathbf{j}_s is the current density inside the superconductor, λ is the field penetration depth, ξ is the coherence length, $\lambda = \varkappa \xi$. The order parameter, in a general case, is written as $\Psi = \psi e^{i\Theta}$, where ψ is the modulus and Θ is the phase of the order parameter. From the single-valuedness of Ψ the condition follows

$$\oint_C \nabla \Theta d\mathbf{l} = 2\pi m,$$

where the contour C embraces the vortex axis, m is integer (the topological invariant, or fluxoid, or vorticity), which shows, how many vortices may be present inside the contour R .

In the cylindrical system of co-ordinates r, φ, z , with z axis directed along the cylinder element [when the vector-potential has only one component, $\mathbf{A} = \mathbf{e}_\varphi A(r)$], these equations may be written in the dimensionless form

$$\frac{d^2 U}{d\rho^2} - \frac{1}{\rho} \frac{dU}{d\rho} - \psi^2 U = 0, \quad (1)$$

$$\frac{d^2 \psi}{d\rho^2} + \frac{1}{\rho} \frac{d\psi}{d\rho} + \varkappa^2 (\psi - \psi^3) - \frac{U^2}{\rho^2} \psi = 0. \quad (2)$$

Here, instead of the dimensioned potential A , field B and current j_s , the dimensionless quantities $U(\rho)$, $b(\rho)$ and $j(\rho)$ are introduced:

$$A = \frac{\phi_0}{2\pi\lambda} \frac{U + m}{\rho}, \quad B = \frac{\phi_0}{2\pi\lambda^2} b, \quad b = \frac{1}{\rho} \frac{dU}{d\rho}, \quad (3)$$

$$j(\rho) = j_s / \frac{c\phi_0}{8\pi^2\lambda^3} = -\psi^2 \frac{U}{\rho}, \quad \rho = \frac{r}{\lambda}.$$

(The field B in (3) is normalized by $H_\lambda = \phi_0/(2\pi\lambda^2)$, with $b = B/H_\lambda$; instead of H_λ one can normalize by $H_\xi = \phi_0/(2\pi\xi^2) \equiv H_{c2}$ [28–30], or by thermodynamical critical field $H_c = \varkappa H_\lambda/\sqrt{2}$. The coefficients in (1)–(3) would change accordingly.)

The magnetic flux, confined inside the contour of the radius r , is

$$\Phi = \int \mathbf{B} ds = \oint_r \mathbf{A} d\mathbf{l} = \phi_0 (U + m), \quad U = U(\rho), \quad \rho = \frac{r}{\lambda}.$$

Thus, the potential $U(\rho)$, in the normalization adopted above, is related to the flux $\Phi(\rho)$ by a simple formula $\phi \equiv \Phi/\phi_0 = U(\rho) + m$.

Because the magnetic flux through the vanishing contour is zero, and the field $B|_{r=R} = H$, the following boundary conditions correspond to Eq. (1):

$$U|_{\rho=0} = -m, \quad \left. \frac{dU}{d\rho} \right|_{\rho=\rho_1} = h_\lambda, \quad (4)$$

where $\rho_1 = R/\lambda$, $h_\lambda = H/H_\lambda$, $H_\lambda = \phi_0/(2\pi\lambda^2)$.

As to the Eq. (2), we shall take the usual boundary condition on the external surface [1]: $d\psi/d\rho|_{\rho=\rho_1} = 0$. The order parameter at the center is either maximal (if $m = 0$), or zero (if $m > 0$, see, for instance, [29]), thus, the following boundary conditions correspond to Eq. (2):

$$\left. \frac{d\psi}{d\rho} \right|_{\rho=0} = 0, \quad \left. \frac{d\psi}{d\rho} \right|_{\rho=\rho_1} = 0 \quad (m = 0), \quad (5)$$

$$\psi|_{\rho=0} = 0, \quad \left. \frac{d\psi}{d\rho} \right|_{\rho=\rho_1} = 0 \quad (m > 0). \quad (6)$$

The magnetic moment (or, magnetization) of the cylinder, related to the unity volume, is

$$\frac{M}{V} = \frac{1}{V} \int \frac{B - H}{4\pi} dv = \frac{B_{av} - H}{4\pi}, \quad (7)$$

$$B_{av} = \frac{1}{V} \int B(\mathbf{r}) dv = \frac{1}{S} \Phi_1,$$

where B_{av} is the mean field value inside the superconductor, $\Phi_1 = \Phi(R)$, $S = \pi R^2$. In normalization (3), denoting $\bar{b} = B_{av}/H_\lambda$, $h_\lambda = H/H_\lambda$, $M_\lambda = M/H_\lambda$, one finds from (7):

$$4\pi M_\lambda = \bar{b} - h_\lambda, \quad \bar{b} = \frac{2}{\rho_1^2}(U_1 + m), \quad \phi_1 = \frac{\Phi_1}{\phi_0} = U_1 + m, \\ U_1 = U(\rho_1), \quad \rho_1 = \frac{R}{\lambda}. \quad (8)$$

For the difference of Gibbs free energies of the system in superconducting and normal states, $\Delta G = G_s - G_n$, it is convenient to use the exact expression:

$$\Delta G = \mathcal{F}_{s0} - \frac{1}{2}MH + \frac{\phi_0 Z}{8\pi} m(B(0) - H), \quad (9)$$

$$\mathcal{F}_{s0} = \frac{H_c^2}{8\pi} \int \left[\psi^4 - 2\psi^2 + \xi^2 \left(\frac{d\psi}{dr} \right)^2 \right] dv, \quad H_c = \frac{\phi_0}{2\sqrt{2}\pi\lambda\xi},$$

where \mathcal{F}_{s0} corresponds to the superconductor condensation energy, M is the cylinder magnetic moment, Z is the cylinder length, m is the magnetic quantum number, $B(0)$ is the magnetic field at the cylinder axis, H is the

external magnetic field. The expression (9) follows from the general formula, obtained in [31] for the free energy of a hollow superconducting cylinder, if the radius of a hollow is put to zero (see also [32,33]). Using normalization (3), and also (8), one finds from (9) the normalized expression

$$\Delta g = \Delta G / \left(\frac{H_{cm}^2}{8\pi} V \right) = g_0 - \frac{8\pi M_\lambda}{\varkappa^2} h_\lambda + \frac{4m}{\varkappa^2} \frac{b(0) - h_\lambda}{\rho_1^2}, \quad (10)$$

$$g_0 = \frac{2}{\rho_1^2} \int_0^{\rho_1} \rho d\rho \left[\psi^4 - 2\psi^2 + \frac{1}{\varkappa^2} \left(\frac{d\psi}{d\rho} \right)^2 \right].$$

The expressions (3),(8),(10) will be used in Sec. 3 for calculating the corresponding quantities.

We remind, that the field penetration depth λ and the coherence length $\xi = \lambda/\varkappa$ depend on temperature. Thus, the expressions above depend implicitly on temperature, and, formally, are valid for arbitrary values of T . (Though, the Ginzburg-Landau equations themselves are applicable only in the limit $T \rightarrow T_c$ [34,28–30], when the expression $\xi(T) = \xi_0/\sqrt{1 - T/T_c}$ may be used for the coherence length).

It is appropriate to make here a comment on the iteration procedure, we used to obtain the self-consistent solution of the system of equations (1)–(6). First, some trial function $\psi(\rho)$ was chosen, and the solution for $U(\rho)$ was found from Eqs. (1), (4). Then, this function $U(\rho)$ was introduced into Eq. (2), which was solved with account of the boundary conditions (5), (6) and new function $\psi(\rho)$ was found. Further, Eq.(1) was solved again, and all the procedure was repeated, until the functions $\psi(\rho)$ and $U(\rho)$ ceased to change, representing the self-consistent solution of the system (see also [25,35]). However, the numeric algorithm, used in our calculations, does not allow to find the unstable "superheated" and "supercooled" states in type-I superconductors (with $\varkappa < 1/\sqrt{2}$), where other methods are required (see [32,36,37]).

The question of stability requires an additional illumination. Alongside with the centrally symmetric giant-vortex states, the so-called multi-vortex solutions of the same vorticity m exist. The multi-vortex states correspond to the case, when a single giant vortex (with vorticity m) decays into a number of vortices (with vorticities m_i , $\sum m_i = m$). These vortices can be arbitrary positioned on the cylinder cross-section, so the multi-vortex state may be no longer centrally symmetric. The question, which of these multi-vortex states possesses the minimal free energy, is important, because the physical system is usually assumed to occupy the state with the smallest energy (the equilibrium ground state), and all other states are considered as energetically unstable (or metastable). The free energy calculations to find the equilibrium multi-vortex configuration is a difficult problem, which requires the specific methods of investigation.

(See, for instance, the theory [30], where the triangular lattice of single vortices is found as an equilibrium state for the case of infinite superconductor, placed in the field $H \sim H_{c1}$. The numeric calculations for mesoscopic superconducting discs may be found in [6–15], where a simplified model of the vortex distribution is considered. To find the equilibrium vortex configuration in a general case of a finite-size superconductor, placed in arbitrary magnetic field H , is a problem as yet unsolved.)

In the present work a limited task was set: to describe the formal properties of the giant-vortex states, which were not reported previously (in particular, the edge-suppressed transitions and the jumps in the magnetization curves with a fixed vorticity m). The general problem of energetic stability and of the equilibrium vortex configuration is left outside the scope of the present investigation. Some of the edge-suppressed states, which are described below, might in reality be energetically metastable and decay into an equilibrium ground state configuration. However, as is well known, the physical system not necessarily must be in equilibrium, but (with some probability) may also occupy the excited metastable states. The giant-vortex and the edge-suppressed solutions provide the system this opportunity, so the behavior of a superconductor in such states might be of some interest.

The results of our calculations are presented below.

III. THE NUMERICAL RESULTS

The results of the investigation are illustrated below by a number of graphics, which detalize various aspects of this multy-parameter task. (Some of these results can be obtained by the methods, used in the papers, cited above. However, for the uniformity of presentation, we prefer to reproduce them by our method.)

Evidently, the superconductivity would be destroyed by a large external field H with subsequent transition to the normal state. In Fig. 1(a) the phase diagram is depicted (for $\varkappa = 2$ and different m), which separates the normal (n) and superconducting (s) states on the plane of variables $R_\lambda = R/\lambda$ and $h_\xi = H/H_\xi$. The phase diagram is a many-sheet surface, each sheet corresponds to the fixed value of the vorticity m . The sheet $m = 0$ is the lowest laying (according to the increasing m), the sheet $m = 1$ lays above it, still more above lays the sheet $m = 2$, and so on. (It is sufficient to consider only the values $m \geq 0$, because the results for $m < 0$ are easily reproducible with account of the evident symmetry $(m, H) \iff (-m, -H)$.)

On each of m -sheets of the phase surface there is a phase curve (h_c , which may be marked by the index m), which separates the region of values (R_λ, h_ξ) , where the superconducting solutions exist (i.e. $\psi > 0$), from the region of normal state solutions ($\psi \equiv 0$). For a

bulk superconductor ($R_\lambda \gg 1$) the superconducting state boundary (in the case of type-II superconductor) lays at $h_\xi = H/H_\xi = 1$, i.e. at $H = H_{c2} = \phi_0/(2\pi\xi^2)$ [28–30] ($H_{c2} \equiv H_\xi$). As can be seen from Fig. 1(a), for small R_λ the superconducting states (with different values of m) are also possible in the fields, exceeding the critical value H_{c2} (i.e. for $h_\xi > 1$). For fixed R_λ and m there exists a maximal field $h_\xi = h_c^{(m)}$, above which the superconducting solution is impossible. As is well known, the maximal field, at which the superconductivity is still possible (for a bulk specimen with $R_\lambda \gg 1$) is $h_\xi = 1.69$ (i.e. $H = H_{c3}$, where $H_{c3} = 1.69H_{c2}$ is the field, at which the surface superconductivity nucleates in macroscopic specimens [26–30]). As is evident from Fig. 1(a), for small R_λ , the superconductivity is also possible in the fields, exceeding $h_\xi = 1.69$. [The analogous phase diagram in the case of type-I superconductor (with $\varkappa = 0.5$, $m = 0, 1, 2$) is depicted in Fig. 1(b).]

Inside each of the superconducting regions in Fig. 1(a) there exists a singular line h_s , which is depicted, for clarity, on a separate phase m -sheet (see Fig. 2). In Fig. 2(a) the phase sheet $m = 0$ (for $\varkappa = 2$) is depicted. The solid line h_c corresponds to the superconducting state boundary. The letter s marks the region, where the superconducting state exists ($\psi \neq 0$), the letter n denotes the normal state ($\psi = 0$).

To every point (R_λ, h_ξ) , which lays inside the superconducting region in Fig. 2(a), corresponds some solution of Eqs. (1)–(6). When this point is shifted, the solution changes accordingly. The central part of the drawing (which lays in the withinity of $h_\xi \sim 0$) corresponds to the superconducting Meissner state. The order parameter here is $\psi \sim 1$, the external field H is almost completely screened out and penetrates only to the distance $\sim \lambda$ from the superconductor surface. The shape of the Meissner solution depends on H only slightly.

There exists a critical line h_s in Fig. 2(a), near which the Meissner solution ($\psi \sim 1$) starts to change strongly. The character of this transformation depends on the cylinder radius R_λ . If the representation point (R_λ, h_ξ) crosses the the critical line h_s above the point R_Δ ($R_\lambda > R_\Delta$), the static Meissner solution becomes absolutely unstable relative small variations in its form, and transforms by a jump into new stable (static) superconducting solution with the same m . In this new state (which may be called as "edge-suppressed", or "rim-suppressed" [25]) the order parameter $\psi(r)$ is strongly suppressed in some layer, which is situated near the superconductor surface, while the magnetic field penetrates this layer practically without screening (see Fig. 2 in [25] for $m = 0$ and also Figs. 3–5 below).

The jump transformation of the order parameter shape is accompanied by jumps in the magnetization and in other physical characteristics (see Fig. 3 below). The amplitude of these jumps diminishes with R_λ diminish-

ing, and for $R_\lambda = R_\Delta$ the jump amplitude (see the broken vertical lines in Fig. 3) vanishes. Thus, for $R_\lambda > R_\Delta$ the transition of the Meissner state ($m = 0$) to the edge-suppressed form ($m = 0$) is the first order phase transition (by a jump).

For $R_\lambda < R_\Delta$ the Meissner solution also changes its form significantly, when the line h_s is crossed, but this transformation happens smoothly, without jump (a second order phase transition to the edge-suppressed form). In the case $R_\lambda = R_\Delta$ the jump amplitude is zero, so the first and second order phase transitions to the edge-suppressed state become indistinguishable. (The meaning of the points R_w, R_0, R_Δ in Figs. 2(a, d) will be explained later.)

As was noted, to every point of s -region in Fig. 2(a) corresponds some solution of Eqs. (1)–(6) for functions ψ and U , which describe the superconducting state. When the representation point (R_λ, h_ξ) moves, this state changes. Let us trace in more details, what happens, if the parameter $R_\lambda = R/\lambda$ remains constant (i.e. the temperature remains constant), but the parameter $h_\xi = H/H_\xi$ changes (i.e. only the field H changes).

In Fig. 3 are depicted as functions of H : (a) – the system magnetic moment ($-4\pi M_\lambda$) (8); (b) – the average magnetic field \bar{b} [or, the total magnetic flux inside the cylinder, $\phi_1 = \frac{1}{2}\rho_1^2\bar{b}$] (8); (c) – the difference of the system free energies, Δg , (10); (d) – the magnetic field magnitude at the cylinder axis, b_0 ; (e) – the maximal value of the superconducting order parameter, ψ_{max} ; (f) – the order parameter value at the cylinder surface, ψ_1 . Fig. 3 corresponds to the case $m = 0, \varkappa = 2, R_\lambda = 5$. [The superconducting region in Fig. 2(a) is crossed along the line $R_\lambda = 5$.] The values of $h_\lambda = \varkappa^2 h_\xi$ are plotted on the horizontal axis. By open circles the points are marked, which deserve a special commentary.

As is seen from Fig. 3(a), the magnetic moment ($-4\pi M_\lambda$) increases linearly for small $h_\lambda > 0$ ($h_\lambda = 0$ at the point 4). The average magnetic field inside the cylinder, \bar{b} , is essentially reduced, in comparison to the normal state (see the dotted line n in Fig. 3(b)). (Analogously behaves the total magnetic flux, confined inside the cylinder, ϕ_1). The initial linear part reflects the Meissner effect, it corresponds to the external field expulsion from the superconductor interior. If the field H is increased further, the magnetic moment increases up to the point 5, where the magnetization diminishes by jump, and takes the value 6.

The analogous jumps are present in other quantities, depicted in Figs. 3(b–f). The value of the order parameter at the surface, ψ_1 (Fig. 3(f)), changes especially strongly: from $\psi_1 = 0.706$ at the point 5 (where $h_\lambda = 1.6837$), to $\psi_1 = 0.087$ at the point 6 (where $h_\lambda = 1.6838$). The jump in the free energy Δg (Fig. 3(c)) is not seen in this scale.

When the external field h_ξ is increased beyond the point 6, the maximal value of the order parameter, ψ_{max} ,

starts diminish quickly. This is accompanied by a fast drop in the "tail" of the magnetization. (This "tail" lays between the points 6 and 7 in Fig. 3(a) and represents the edge-suppressed solution, e_0 .) When the field h_ξ reaches the point 7, the order parameter vanishes completely, by the second order phase transition to the normal state ($\psi_{max} \rightarrow 0$).

Fig. 4 ($m = 0, \varkappa = 2$) demonstrates, what is going on, when the cylinder radius R is diminishing. [The superconducting region in Fig. 2(a) is crossed along the line $R_\lambda = 3$.] Now, there are no jumps on the magnetization curve (Fig. 4(a)), which were represented by dashed lines in Fig. 3(a). But, the points of inflection 2 and 4 remain, where the magnetization curve has the maximal derivative. The corresponding points in Figs. 4(b, c) are marked by the same numerals 2 and 4 as in Fig. 4(a). Evidently, the solution transforms smoothly, when the field h_λ passes the critical value h_s (the point 4). This point corresponds approximately to the value R_Δ in Fig. 2(a), where the derivative of the magnetization curve is infinite.

In Fig. 5 the case $m = 0, \varkappa = 2, R_\lambda = 1$ is presented. [The superconducting region in Fig. 2(a) is crossed along the line $R_\lambda = 1$.] Here, the inflection point 4 ($h_\lambda = 5.91$) on the curve ($-4\pi M_\lambda$) practically coincides with the termination point 5 ($h_\lambda = 5.96$). This situation corresponds to the point R_w in Fig. 2(a) (where h_s and h_c merge), and where the tail of the magnetization disappears (i.e. the width of the tail vanish). For $R_\lambda < R_w$ the second order phase transition to the normal state occurs, and the magnetization curve has no tail.

Evidently, the picture, presented by Fig. 2(a) ($m = 0$), is symmetric relative the axis $h_\xi = 0$. The analogous picture, which corresponds to the phase sheet $m = 1$ [Fig. 2(d)], is asymmetric relative the axis $h_\xi = 0$. The edge-suppressed state exists only in the region $h_\xi > 0$, and they do not exist in the region $h_\xi < 0$. This may be interpreted in the physical terms.

The phase sheet $m = 1$ describes situation, when at the cylinder axis there is a single vortex (its own field is assumed to have a positive sign), with the order parameter vanishing on the axis: $\psi_0 = 0$. If the external field of the same direction ($h_\xi > 0$) is applied, the magnetic field is additionally pumped into the specimen. When the field reaches the critical value h_s , the superconductivity is partly destroyed, and a new superconducting state forms, with strongly suppressed order parameter ψ_1 at the cylinder surface (see Fig. 6(f) below). This state preserves up to the field $h_\xi = h_c^{(+)}$ (the right branch of the critical line, $h_c > 0$), until the order parameter vanishes finally everywhere. Thus, in the vicinity of the line $h_c^{(+)}$ in Fig. 2(d), the mechanism of the order parameter suppression by the external field acts.

If the external field has the opposite sign [$h_\xi < 0$, Fig. 2(d)], the field of the vortex ($m = 1$) is gradual pumped

out from the vortex interior. When the external field reaches the critical value $h_\xi = h_c^{(-)}$ (the left branch of the critical line, $h_c < 0$), the vortex magnetic field b_0 is completely sucked out from the superconductor (see Fig. 6(d)). When this happens, the vortex field at the axis vanishes (this means the jump transition from the state $m = 1$ to the state $m = 0$); the order parameter also vanishes by a jump (see Figs. 6(e, f)). Thus, in the vicinity of the line $h_c^{(-)}$, the mechanism of pumping out the field from the vortex interior acts. This explains the asymmetric behavior of the curves $h_c^{(-)}$ and $h_c^{(+)}$ in Fig. 2(d).

Note also, that the curves $h_c^{(-)}$ and $h_c^{(+)}$ come up to the axis $h_\xi = 0$, having different derivatives (the fracture point at $h_\xi = 0$ is marked by an open circle in Fig. 2(d); the corresponding value at R_λ -axis is R_0).

Mention one more peculiarity of the curves, depicted in Fig. 2(d). In the case of small radii (for $R_\lambda < R_0$ and $m = 1$) there exists a field interval, where the superconducting state, which was impossible at smaller h_ξ , becomes possible again for larger h_ξ . Here one has an example of the so-called "reentry" superconductivity. In a cylinder of very small radius ($R_\lambda < R_0$) the magnetic field of the vortex can not be confined inside the superconductor and dissipates outside through the cylinder surface. However, the imposition of the external field prevents the dissipation of the vortex field and stabilizes the superconducting state. If the external field is increased further, the superconductivity will be finally destroyed. Thus, on the lowest part of the curve h_c in Fig. 2(d) there exists a minimum at $R_\lambda = R_{\lambda min}$ (marked by an open circle).

If the parameter \varkappa is increased, the curves h_s and h_c behave analogously to what is shown in Figs. 2(a, d). But, if \varkappa diminishes (see Figs. 2(b, e)), the point, where the curves h_s and h_c merge, raises up to larger R_λ , and the width of the region, where the edge-suppressed state exists, diminishes. At $\varkappa = 1/\sqrt{2}$ the width of this region vanishes, and the curves h_s and h_c merge into one indivisible curve h_c . For $\varkappa < 1/\sqrt{2}$ (i.e. for type-I superconductors) the edge-suppressed states do not exist. The behavior of the critical curves h_c in the case of type-I superconductor is depicted in Fig. 2(c, f) for different $\varkappa < 1/\sqrt{2}$ ($m = 0$ and 1). One can see, that the superconducting state with a vortex ($m = 1$) at the cylinder axis, in principle, can exist in both type-I and type-II superconductors.

The solution behavior in a case $m = 1$, $\varkappa = 2$ [when the superconducting region s in Fig. 2(d) is crossed along the line $R_\lambda = 5$] is illustrated in Fig. 6. There are also jumps, as in Fig. 3, but the curves are asymmetric relative the axis $h_\xi = 0$. In particular, on the magnetic moment curve (Fig. 6(a)), in a case $h_\lambda < 0$ there is no "tail", which exists in Fig. 3(a) for $h_\lambda < 0$ (between points 1 and 2). This asymmetry (as was already mentioned) may

be explained by different mechanisms, which act in destruction of the superconducting state $m = 1$. If $H > 0$, the additional pumping of the external field into the superconductor occurs, with the subsequent suppression of the order parameter by the field, followed by the transition to the normal state (or, to the state $m \rightarrow m + 1$). If $H < 0$, the field is pumped out from the vortex and the superconductor passes into the vortex-free state $m = 0$ (or, even into the normal state).

The analogous picture (for $m = 1$, $\varkappa = 2$, $R_\lambda = 3$) is presented in Fig. 7. In difference to Fig. 4 ($m = 0$), the curves in Fig. 7 ($m = 1$) have no smooth "tails" for $h_\xi < 0$ (to the left of points 2), but they terminate by a jump at the points 2, where the field at the vortex axis, b_0 , vanishes, and the order parameter suffers a jump.

Fig. 8 corresponds to the case $m = 1$, $\varkappa = 2$, $R_\lambda = 1$. Notice, that in Fig. 8(a), at positive values $h_\lambda > 0$ (in the interval between the points 3 and 4) the magnetic moment is positive ($4\pi M_\lambda > 0$), which corresponds to the paramagnetic susceptibility. In the interval between the points 5 and 6 the magnetic moment is negative ($4\pi M_\lambda < 0$), which corresponds to the diamagnetic susceptibility. As can be seen from Fig. 8(b), in the interval between points 3 and 4, the external field enhances the superconductivity (because ψ_{max} increases). In the interval between points 4 and 5, the external field suppresses the superconductivity (because ψ_{max} decreases).

The analogous dependencies are presented in Fig. 9 for type-I superconductor ($R_\lambda = 5$, $\varkappa = 0.5$, $m = 0, 1$). The singular points are marked by an open circles. There are no "tails" on the magnetization curves (Fig. 9(a)) in both regions $h_\xi < 0$ and $h_\xi > 0$. This is characteristic for type-I superconductors with $\varkappa < 1/\sqrt{2}$, when the destruction of the superconductivity by the magnetic field proceeds in a jump, as the first order phase transition. [This is valid, if $R_\lambda > R_\Delta$ in Fig. 1(b). If $R_\lambda < R_\Delta$, the phase transition to the normal state is of second order, even in type-I superconductors; see Fig. 14 below.]

There are other features, common to all type-I superconductors. Thus, if the family of curves, depicted in Fig. 2(e) (for $m = 0$ and different $\varkappa < 1/\sqrt{2}$), is re-drawn on the (R_ξ, h_ξ) -plain, one obtains the unified phase curve, Fig. 10(a) ($m = 0$). Notice also, that in the case $m = 0$ the curves with $\varkappa < 1/\sqrt{2}$ and $\varkappa \geq 1/\sqrt{2}$ almost coincide, so the phase curves in Fig. 10(a) look like one universal function. (For $h_\xi > 1$ this function is $R_\xi \approx 2.8/h_\xi$).

Analogously, if the family of curves in Fig. 2(f) is re-drawn on the (R_ξ, h_ξ) -plain, the Fig. 10(b) emerges. One can see from this figure, that for all $\varkappa \leq 1/\sqrt{2}$ there exists a minimal radius $R_{\xi min} \approx 1.3$. For $R_\xi < R_{\xi min}$ the superconducting state with a vortex ($m = 1$) on the cylinder axis is impossible.

In Fig. 10(b) ($m = 1$), among others, the phase diagrams are depicted for $\varkappa \geq 1$. The corresponding curves (for $h_\xi > 0$ and $R_\xi \gg 1$) have the asymptote $h_\xi = 1$

(or $H = H_{c2}$), common to all type-II superconductors with $\varkappa \geq 1$ (see Figs. 1 and 2). However, if $\varkappa < 1$, these asymptotes depend on \varkappa and began deviate from the value $h_\xi = 1$. [Thus, $h_\xi \rightarrow 1$ for $\varkappa = 1$; $h_\xi \rightarrow 1.058$ for $\varkappa = 0.9$; $h_\xi \rightarrow 1.218$ for $\varkappa = 0.8$; $h_\xi \rightarrow 1.416$ for $\varkappa = 1/\sqrt{2}$.] This means, that in the case $m = 1$ the value $\varkappa = 1$ is singular for equations (1)–(6). At this value the solution passes from one branch ($\varkappa \geq 1$) to another ($\varkappa < 1$). At the same time, the value $\varkappa = 1/\sqrt{2}$ is also singular, because at $\varkappa = 1/\sqrt{2}$ the second branch of solutions appears (or vanishes), which describe the edge-suppressed states [compare the behavior of the curves h_s in Figs. 2(a–e)].

Now, we present the examples of concrete solutions of Eqs. (1)–(6), as functions of the space coordinate $\rho = r/\lambda$ ($0 \leq r \leq R$) for $m = 1$. (The solutions profiles for the vortex-free state ($m = 0$) are shown in [25], Fig. 2.)

In Fig. 11 the solutions are shown in the case $R_\lambda = 5$, $m = 1$, for several values of h_λ . Note the curve 3 in Fig. 11(a), which corresponds to $h_\lambda = 0$ and describes a screened Meissner-type vortex state v_1 ($m = 1$). (In Fig. 6(a) to this state corresponds the point 4.) The curve 4 in Fig. 11(a) corresponds to the point 5 in Fig. 6(a), where $h_\lambda = 1.8254$. Here the solution branch v_1 terminates, the temporal instability develops, and at $h_\lambda = 1.8255$ the solution passes to new stable (static) branch e_1 (the edge-suppressed state $m = 1$, the point 6 in Fig. 6(a)). The curve 5 in Fig. 11(a) corresponds to the value $h_\lambda = 1.8255$ and describes the edge-suppressed state e_1 with a vortex ($m = 1$) at the cylinder axis (here $\psi(0) = 0$ and the order parameter is additionally strongly suppressed near the cylinder surface).

It is expedient to trace in more details the system behavior in the states with different m , when the cylinder radius R is fixed, and only the external field H varies. If the superconducting region in Fig. 1(a) is crossed along the line $R_\lambda = 2$, the states with $m = 0, 1, 2, \dots, 11$ are possible. These states are represented in Fig. 12 by the following dependencies: (a) – the normalized free-energy difference (Δg); (b) – the magnetization ($-4\pi M_\lambda$); (c) – the maximal value of the order parameter (ψ_{max}) in the state m .

In Fig. 12(a) the free-energy curves with the adjacent m -values intersect at the points, marked by the open circles. At these points the equilibrium transitions from the state m to the lower energy state $m+1$ (or reversed) may occur. Such equilibrium transitions are accompanied by the reversible jumps in the magnetization (see the broken vertical lines in Fig. 12(b)). Thus, the equilibrium magnetization curve should be reversible and have a characteristic saw-like shape. Note also, that in the case of equilibrium transitions the magnetization should be positive for all external fields ($-4\pi M_\lambda > 0$), this corresponds to the diamagnetic susceptibility. [The Meissner state with $m = 0$ is always diamagnetic.]

However, if the metastable states with $m > 0$ are also

admissible (i.e. those parts of curves in Fig. 12(a), which lay to the left of the intersection points), then the magnetization may turn negative within some field interval ($-4\pi M_\lambda < 0$ for $m \geq 1$), this corresponds to the paramagnetic susceptibility. The magnetization curve in this case might be irreversible and display the hysteresis behavior.

Note also, that some of the magnetization curves in Fig.12(b) ($R_\lambda = 2$) have smooth "tails" (for instance, at $m = 0$), what indicates to the presence of the edge-suppression effect. For larger radii ($R_\lambda > R_\Delta \sim 4$), instead of the inflection points, the reversible jumps in the magnetization may appear, which are analogous to those in Fig. 6(a). Probably, such qualitative details may be seen in the experiments with mesoscopic samples.

As is evident from Fig. 12(c), each of the superconducting m -states can exist only within a limited interval of fields, where $\psi_{max} > 0$. When the field h_ξ is increased, only the last state (with $m = 11$) survives. In this state the superconducting region with $\psi \neq 0$ is maximally pushed toward the cylinder surface, but the interior is almost normal (see Fig. 13 below). Evidently, the state with $m = m_{max}$ is just the state of the surface superconductivity [26,27]. In a massive cylinder ($R_\lambda \gg 1$) the last traces of the superconductivity may persist up to the field $h_\xi = 1.69$ [or, the third critical field $H = H_{c3} = 1.69H_{c2}$]. At smaller R_λ the superconductivity may persist in the fields, which exceed H_{c3} (see Fig. 1(a)).

A peculiar field-compression effect is also present in Fig. 12. The first superconducting solution, which appears in a field-cooled regime, has maximal possible m (the state of the surface-enhanced superconductivity). When the external field diminishes, this state becomes impossible, but new $m-1$ -state appears, in which the superconducting region is shifted toward the center, and simultaneously the edge-suppressed region begins to form. The state $m = 4$, for instance, has both the region of edge-suppressed superconductivity (where the external field is practically not screened), and the region at some distance from the center, where the field of the giant vortex ($m = 4$) is compressed and the superconductivity is also almost crushed (because at the center the order parameter is always small, $\psi(\rho) \sim \rho^m \ll 1$). (A flux-compression effect was discussed also in [6]).

As was mentioned, Fig. 12(b) indicates to the possible paramagnetic susceptibility of the superconducting cylinder in the state with $m > 0$. This topic also deserves a special comment.

The paramagnetic Meissner effect (or, Wohlleben effect) was initially observed in [40] and extensively discussed in the literature (see, for example, Refs. [6,8,11,15,41-43] and references therein). A number of controversial explanations of this effect were proposed, but there is as yet no clear understanding of its nature. This effect is observed, in particular, in a finite-dimension samples, in the field-cooled regime, it shows the signs of

metastability, of the reentrant behavior and hysteresis [43]. It is interesting, that all these features follow naturally from Eqs. (1)–(6) of the Ginzburg–Landau theory.

Consider, for instance, the state $m = 4$ (which is distinguished, for clarity, by thick curves in Fig. 12). This state can not exist in small external fields h_ξ , because the vortex magnetic field ($m = 4, R_\lambda = 2$) is too strong for a mesoscopic sample, and can not be confined inside. However, the imposition of a finite external field prevents the field dissipation, the situation stabilizes and the state $m = 4$ becomes possible again in a larger field (the reentrance effect). Evidently, it is more easy to occupy the state $m = 4$, going down from the stronger fields h_ξ (in a field-cooled regime). The negative part of the magnetization curve $m = 4$ (the paramagnetic branch) corresponds to a metastable state of higher free-energy (see Fig. 12. (a)), than the state $m = 3$. [Here the state $m = 4$ is defined as metastable, on the ground, that its free energy is less than the free energy of the state $m = 3$. Such metastability means, that the irreversible transition to the lower laying state $m = 3$ is possible. However, the state $m = 4$ continues to be stable relative small perturbations of its form.]

Note, that in the positive part of the magnetization curve the superconducting currents flow, mainly, to screen out the external field. [This leads to the diamagnetic response in Fig. 12(b).] In the negative part of the magnetization curve the role of the vortex field is more important, and the superconducting screening currents flow, mainly, in the opposite direction. [This means the sign reversion of the magnetic moment, because it is proportional to the current, $\mathbf{M} \sim \int [\mathbf{j}_s \mathbf{r}] dv$. The presence of positive and negative contributions to the total magnetic moment is evident also from Fig. 11(f), where the current density may be positive or negative). At the point $M_\lambda = 0$ the currents, which screen the internal and external fields, counterbalance each other. Thus, according to the Ginzburg–Landau theory, the paramagnetism present in Fig. 12, has purely electrodynamic explanation.

Now we shall demonstrate, how the order parameter vanishes in approaching the critical curves $h_c^{(m)} > 0$ in Figs. 1 and 2 [the curves h_c are supplied with an additional index (m)]. The order parameter is small in the vicinity of $h_c^{(m)}$. In Fig. 13 the degenerated solutions (i.e. those with $\psi_{max} \ll 1$) are shown for $R_\lambda = 2$, $\varkappa = 2$ and different m . [The curves in Fig. 13 are normalized to unity, with true values $\psi_{max} \ll 1$.] In the origin of coordinates the order parameter behaves as $\psi(\rho) \sim \rho^m$, in agreement with the theory (see, for instance, [29,35]). At $\rho \gg 1$ the order parameter is also small (here the edge-suppressed state e_m is formed). For all degenerated solutions, depicted in Fig. 13 (with $\psi_{max} \ll 1$), the field $B(r) \approx H$. In this case Eqs. (1),(2) can be linearized and reduced to one linear equation for the function ψ [26,27]. The solutions of this equation may be found

analytically, in terms of the Kummer functions (see, for instance, [6,8]). [Notice, however, that the normalization factor in the linear equation for ψ remains arbitrary, and to find the true value ψ_{max} it is necessary to solve the full system of nonlinear equations (1)–(6).] The critical fields $h_c^{(m)} > 0$ in Fig. 1, which we found by solving the full system of equations (1)–(6), may be obtained more easily on the base of a linear equation (when $\psi_{max} \ll 1$), as was done in [6,8]. [However, when approaching the phase boundaries $h_c^{(m)}$ for negative $h_\xi < 0$, or to find the critical fields $h_s^{(m)}$, when the edge-suppressed state forms (see Figs. 1 and 2), but the order parameter ψ_{max} remains finite, it is necessary to use the full system of equations (1)–(6).]

It is evident from Fig. 13, that even the degenerated solutions (with $\psi_{max} \ll 1$) display the presence of the edge-suppression effect. If $m = m_{max}$, the order parameter is maximal at the cylinder surface. For $m < m_{max}$ the order parameter begins being suppressed at the boundary. When the field H diminishes, only the states with relatively small m survive [with the inflexion points on the magnetization curves, see Figs. 12(b,c)], and finally the edge-suppressed solutions would form [analogous to those, shown in Fig. 11, with the characteristic jumps, as in Figs. 3 and 6].

Finally, it is of interest to note, that the transitions between states with different m are also possible in type-I superconductors (see also [35,11]). This is demonstrated by Fig. 14. In Figs. 14(a,b) the profiles of the self-consistent solutions $\psi(r)$ and $b(r)$ are shown for type-I superconductor ($\varkappa = 0.5$, $R_\lambda = 4$) in the fields: $h_\xi = 1.4892$ ($m = 0$); $h_\xi = 2.0344$ ($m = 1$); $h_\xi = 2.1084$ ($m = 2$). These h_ξ -values are in the immediate vicinity of the corresponding critical curves $h_c^{(m)}$ in Fig. 1(b): if h_ξ is increased by $1 \cdot 10^{-4}$ [i.e., if the critical curves in Fig. 1(b) are crossed along the line $R_\lambda = 4$], the transitions to the normal state occurs ($\psi(r) = 0$, $B(r) = H$).

As is clear from Fig. 14(a), in type-I superconductors the transition to the normal state is of the first order (by a jump from a finite value ψ_{max}^*). However, the jump amplitude (i.e. the value ψ_{max}^* at the transition point) depends on parameters m , \varkappa and R_λ (or $R_\xi = R_\lambda/\varkappa$). The jump amplitude, $\psi_{max}^*(R_\lambda)$, is depicted in Fig. 14(c) for $\varkappa = 0.1$ and $\varkappa = 1/\sqrt{2}$ in the case $m = 0$. As follows from Fig. 14(c), the value ψ_{max}^* diminishes, when R_λ diminishes, with the jump amplitude vanishing at the point R_Δ . Thus, the points R_Δ on the critical curves in Figs. 1(b), 10(a) and 14(c) divide two regions of the phase transitions in the case of type-I superconductors: for larger $R_\lambda > R_\Delta$ the first order phase transition to the normal state occurs; for smaller $R_\lambda < R_\Delta$ one has the second order phase transition. At $R_\lambda = R_\Delta$ both transitions became indistinguishable, because the jump amplitude ψ_{max}^* vanish. [Remind, that in type-II superconductors, with $\varkappa > 1/\sqrt{2}$, the phase transition to the normal state

is always second order, regardless of the specimen size.] The critical size R_Δ , which separates the regions of the first and second order phase transitions in the case of type-I superconductors, may also be found from different considerations [1,32,36,38]. Fig. 14(c) shows, that this size depends slightly on \varkappa .

IV. COMMENTS AND CONCLUSIONS

In conclusion, the main results of the present investigation are formulated.

The self-consistent solutions of a nonlinear system of Ginzburg–Landau equations, which correspond to the fixed values of the magnetic quantum number m and have a cylinder symmetry (i.e. depend only on the radial coordinate r , but not on the azimuthal angle φ), are studied.

It is found, that for type-II superconducting cylinder of finite radius ($R > R_\Delta$), placed in sufficiently weak magnetic field H , the order parameter $\psi(r) \approx \text{const}$ near the cylinder surface, and behaves as $\psi(r) \sim r^m$ near the center (the giant-vortex state). If the field is increased ($H > H_s^{(m)}$), the giant-vortex state changes abruptly and acquires new form. (A first order phase transition to the edge-suppressed state occurs.) In this new state the order parameter is strongly suppressed near the cylinder edge, with the magnetic field penetrating practically without screening into some layer in the vicinity of the surface. At the center the behavior $\psi(r) \sim r^m$ remains. This transition to the edge-suppressed form is accompanied by jumps in the magnetization and in the total magnetic flux, confined in the cylinder. The properties of such edge-suppressed solutions (which depend on the parameters m, H, \varkappa, T) are studied. It is shown, that the edge-suppressed states exist only in type-II superconductors, but the giant-vortex states are possible both in type-I and type-II superconductors. The phase boundaries are found, inside which the giant m -vortex solutions can exist. In particular, the characteristic radius of the cylinder is found, R_Δ , which separates the regions of the first and second order phase transitions between the superconducting and normal states.

The behavior of the magnetization (M) and of the total magnetic flux (Φ_1) as functions of the external field (H) is found, with account of the jumps, which accompany the formation of the edge-suppressed states. It is demonstrated, that some maximal value $m = m_{max}$ exist, for which the edge-suppressed state degenerates into the usual state of the surface superconductivity (with nucleation field $H \approx H_{c3}$ [26,27]). The Gibbs free energies of different axially symmetrical superconducting states are compared, and the problem of paramagnetic effect, observed in mesoscopic samples, is shortly discussed. It is found, that the paramagnetic effect is possible in metastable vortex states and it may be attributed

to the disbalance of the superconducting currents, which screen the external field H and the field of the vortex from entering the sample interior.

As was pointed out earlier [25], according to the Ginzburg–Landau theory, two competing mechanisms of the external field penetration into the superconducting cylinder exist – in a form of vortices [2–15,30], and in a form of the edge-suppressed layer. The question, which of these mechanisms is more favorable energetically, may be answered only after the full comparison is made of the Gibbs free energies for the arbitrary multi-vortex configurations in a finite radius cylinder. This difficult theoretical problem (as well as the generalisation to other geometries) is left outside the scope of the present investigation. Some of the edge-suppressed states, described above, are metastable, but they may be observable in a specially arranged experiments. We believe it is expedient to draw attention to this possibility.

V. ACKNOWLEDGMENTS

We are grateful to V. L. Ginzburg for the interest to this work and valuable discussions.

-
- [1] V.L. Ginzburg, L.D. Landau, Zh. Exp. Teor. Fyz. **10**, 1064 (1950).
 - [2] H.J. Fink, Phys. Rev. Lett. **14**, 309 (1965).
 - [3] H.J. Fink, A.G. Presson, Phys. Rev. **151**, 219 (1966); Phys. Rev. **168**, 319 (1968).
 - [4] F. de la Cruz, H.J. Fink, J. Luzuriaga, Phys. Rev. B **20**, 1947 (1979).
 - [5] Yu.N. Ovchinnikov, Sov. Phys. JETP **52**, 755 (1980).
 - [6] V.V. Moshchalkov, X.G. Qiu, V. Bruyndoncx, Phys. Rev. B **55**, 11793 (1997).
 - [7] P.S. Deo, V.A. Schweigert, F.M. Peeters, A.K. Geim, Phys. Rev. Lett., **79**, 4653 (1997).
 - [8] V.A. Schweigert, F.M. Peeters, Phys. Rev. B **57**, 13817 (1998).
 - [9] V.A. Schweigert, F.M. Peeters, P.S. Deo, Phys. Rev. Lett. **81**, 2783 (1998).
 - [10] V.A. Schweigert, F.M. Peeters, Phys. Rev. Lett. **83**, 2409 (1999).
 - [11] P.S. Deo, F.M. Peeters, V.A. Schweigert, Supralatt. and Microstruct. **25**, 1195 (1999); Phys. Rev. B **59**, 6039 (1999).
 - [12] V.V. Moshchalkov, Sol. State Com. **78**, 711 (1997).
 - [13] A.I. Buzdin, Phys. Rev. B **47**, 11 416 (1993).
 - [14] A.I. Buzdin, J.P. Brison, Physics Lett. A **196**, 267 (1994).
 - [15] J.J. Palacios, Phys. Rev. B **58**, R5948 (1998); Physica B **256–258**, 610 (1998); Phys. Rev. Lett. **84**, 1796 (2000).
 - [16] G. Dolan, J. Low Temp. Phys. **15**, 133 (1974).
 - [17] O. Buisson et al., Phys. Lett. A **150**, 36 (1990).
 - [18] V.V. Moshchalkov et al., Nature (London) **373**, 319

(1995).

- [19] A.K. Geim, S.V. Dubonos et al., Nature (London) **390**, 259 (1997).
 [20] A.K. Geim, I.V. Grigorieva et al., Nature (London) **396**, 144 (1998).
 [21] A.K. Geim et al., Appl. Phys. Lett. **71**, 2379 (1997).
 [22] A. Bezryadin, B. Pannetier, J. of Low Temp. Phys. **102**, 73 (1996).
 [23] R. Benoist, W. Zwerger, Z. Phys. B**103**, 377 (1997).
 [24] C.A. Bolle et. all., Nature **399**, 43 (1999).
 [25] G.F. Zharkov, V.G. Zharkov, A.Yu. Zvetkov, Phys. Rev. B**61**, 12 293, (2000).
 [26] D. Saint-James, P. de Gennes, Phys. Lett. **7**, 306 (1963).
 [27] D. Saint-James, Phys. Lett. **15**, 13 (1965).
 [28] P.G. de Gennes, *Superconductivity of Metals and Alloys* (Addison-Wesley, New York, 1989).
 [29] M. Tinkham, *Introduction to Superconductivity* (McGraw Hill, New York 1975).
 [30] A.A. Abrikosov, *Fundamentals of the Theory of Metals* (North-Holland, Amsterdam, 1988).
 [31] R.M. Arutyunian, V.L. Ginzburg, G.F. Zharkov, Zh. Exp. Teor. Fyz. **111**, 2175 (1997) [JETP **84**, 1186 (1997)].
 [32] V.L. Ginzburg, Zh. Exp. Teor. Fyz. **34**, 113 (1958).
 [33] R.M. Arutunian, G.F. Zharkov, J. Low Temp. Phys. **52**, 409 (1983).
 [34] L.P. Gor'kov, Zh. Exp. Teor. Fyz. **37**, 1918 (1969).
 [35] G.F. Zharkov, V.G. Zharkov, Physica Scripta **57**, 664 (1998).
 [36] H.J. Fink, D.S. McLachlan and B. Rothberg-Bibby, in *Prog. in Low Temp. Phys.*, v. VIIIb, p. 435–516, ed. D. F. Brewer, North Holland Pub., Amsterdam- New York- Oxford (1978).
 [37] A.J. Dolgert, S.J. DiBartollo and A.T. Dorsey, Phys. Rev. B **53**, 5650 (1996).
 [38] V.P. Sylin, Zh. Exp. Teor. Fyz. **21**, 1330 (1951).
 [39] W. Buckel, *Supraleitung. Grundlagen und Anwendungen* (Berlin, Akad.-Verl., 1973).
 [40] W. Braunish, N. Knauf et. all., Phys. Rev. B **48**, 4030 (1993).
 [41] A.E. Koshelev, A.I. Larkin, Phys. Rev. B **52**, 13 559 (1995).
 [42] J.J. Palacios, Phys. Rev. Lett. **84**, 1796 (2000).
 [43] B. Muller-Alinger, A.C. Motta, Phys. Rev. Lett. **84**, 3161 (2000).

Figures captions

Fig. 1. (a) – The phase diagram of type-II superconductor ($\varkappa = 2$). The numerals at the curves – the values of the magnetic quantum number m . The value $h_\xi = 1$ corresponds to the critical field $H_{c2} = \phi_0/(2\pi\xi^2)$. The value $h_\xi = 1.69$ corresponds to the maximal field $H_{c3} = 1.69H_{c2}$, in which the surface superconductivity is still possible in macroscopic specimens. (b) – The phase diagram of type-I superconductor ($\varkappa = 0.5$, $m = 0, 1, 2$). The arrows and the letter R_Δ at the curves denote the points, where the first and second order phase transitions to the normal state became indistinguishable (see the text).

Fig. 2. (a) – The case $m = 0$, $\varkappa = 2$. The phase curve h_c divides superconducting (s) and normal (n) states of the cylinder. When the representation point (R_λ, h_ξ) crosses the line h_s (the dotted line), a new edge-suppressed solution forms, with suppressed order parameter ψ_1 (see Fig. 3(f)). No edge-suppressed states exist for $R_\lambda < R_w$. (d) – Analogously, for the case $m = 1$, $\varkappa = 2$. When $R_\lambda < R_0$, the field $h_\xi > 0$ stimulates the superconducting state, so the reentry superconductivity is possible. (b) and (e) – Analogously, for different $\varkappa \geq 1$. (c) and (f) – The phase curves of type-I superconductor (for various $\varkappa \leq 1/\sqrt{2}$). The edge-suppressed states in type-I superconductors are absent.

Fig. 3. The case $m = 0$, $\varkappa = 2$, $R_\lambda = 5$. (a) – The cylinder magnetic moment, $M_\lambda = M/H_\lambda$. (b) – The average magnetic field in the cylinder, \bar{b} (or, the total magnetic flux in the system, $\phi_1 = \frac{1}{2}\rho_1^2\bar{b}$ (8)). (c) – The normalized difference of free energies, Δg , (10). (d) – The magnetic field at the cylinder axis, b_0 . (e) – The maximal value of the order parameter, ψ_{max} . (f) – The order parameter at the cylinder surface, ψ_1 . The letter v_0 denotes the Meissner state (vortex-free, $m = 0$). The letter e_0 denotes the edge-suppressed state (vortex-free, $m = 0$). The transition from one branch of the solution to another takes place between points 2,3, or 5,6. (The solution profiles for the case $R_\lambda = 5$, $m = 0$, $\varkappa = 2$ are depicted in [17], Fig.2.)

Fig. 4. Analogous to Fig. 3, but for the case $m = 0$, $\varkappa = 2$, $R_\lambda = 3$.

Fig. 5. Analogous to Fig. 3, but for the case $m = 0$, $\varkappa = 2$, $R_\lambda = 1$.

Fig. 6. The same, as in Fig. 3, but for $m = 1$, $\varkappa = 2$, $R_\lambda = 5$. The letter v_1 denotes the Meissner-type vortex state (with a vortex $m = 1$ at the cylinder axis). The letter e_1 denotes the edge-suppressed state with the vortex ($m = 1$) at the axis. (The solutions profiles in the case $m = 1$, $\varkappa = 2$, $R_\lambda = 5$, are shown below in Fig. 11.)

Fig. 7. Analogous to Fig. 3, but for the case $m = 1$, $\varkappa = 2$, $R_\lambda = 3$.

Fig. 8. Analogous to Fig. 3, but for the case $m = 0$, $\varkappa = 2$, $R_\lambda = 1$.

Fig. 9. The same, as in Fig. 3, but for type-I superconductor ($\varkappa = 0.5$, $R_\lambda = 5$, $m = 0$ and $m = 1$). There are no edge-suppressed states and no "tails" in the magnetization for type-I superconductors.

Fig. 10. (a) – The phase diagram for $m = 0$ and different \varkappa . The arrow and letter R_Δ divide the regions of the first and second order phase transitions to the normal

state in the case of type-I superconductors. For $m = 0$ the curves with different \varkappa [see numbers in Fig. 10(a)] practically coincide. (b) – The phase diagram for $m = 1$ and different \varkappa . For $R_\xi < R_{\xi min}$ the superconducting state with the vortex ($m = 1$) at the axis is impossible.

Fig. 11. The coordinate dependence of solutions for $m = 1$, $R_\lambda = 5$, $\varkappa = 2$ and different fields (see the values in Fig. 11(a)). (a) – The order parameter, $\psi(\rho)$; $\rho = r/\lambda$. (b) – The derivative, $d\psi/d\rho$. (c) – The second derivative, $d^2\psi/d\rho^2$. (d) – The field potential, $U(\rho)$. (e) – The normalized magnetic field, $b(\rho)$. (f) – The normalized current, $j(\rho)$.

Fig. 12. (a) – The free energy, Δg ; (b) – the magnetic moment, $(-4\pi M_\lambda)$ and (c) – the maximal value of the order parameter, ψ_1 , for the cylinder with $R_\lambda = 2$, $\varkappa = 2$ and various m , as functions of h_ξ .

Fig. 13. The order parameter profiles in a case of degenerated states ($\psi_{max} \ll 1$) for $R_\lambda = 2$, $\varkappa = 2$ and various m . (All the curves represent the self-consistent solutions of Eqs. (1)–(6), but they are normalized to unity.) With m increasing, the value ψ_{max} approaches the boundary $r = R$. The last of the degenerated states ($m = 11$), which is maximally pushed toward the boundary, corresponds to the state of the surface superconductivity [26,27].

Fig. 14. (a) – The order parameter profiles in a case of type-I superconductor ($\varkappa = 0.5$, $R/\lambda = 4$). The external fields (see the numerals at the curves) are in the immediate vicinity of the critical boundaries $h_c^{(m)}$ in Fig. 1(b). If the field h_ξ is increased by $1 \cdot 10^{-4}$, the jump transition to the normal state occurs. (b) – The corresponding magnetic field profiles. (c) – The jump amplitude, ψ_{max}^* , as function of R_λ for $\varkappa = 0.1$ and $\varkappa = 1/\sqrt{2}$. [The jump amplitude ψ_{max}^* is the value of ψ_{max} in a field, which just precedes the first order phase transition to the normal state. The value R_Δ , where the jump amplitude vanish (see Figs. 1(b), 10(a), 14(c)) depends on \varkappa .]

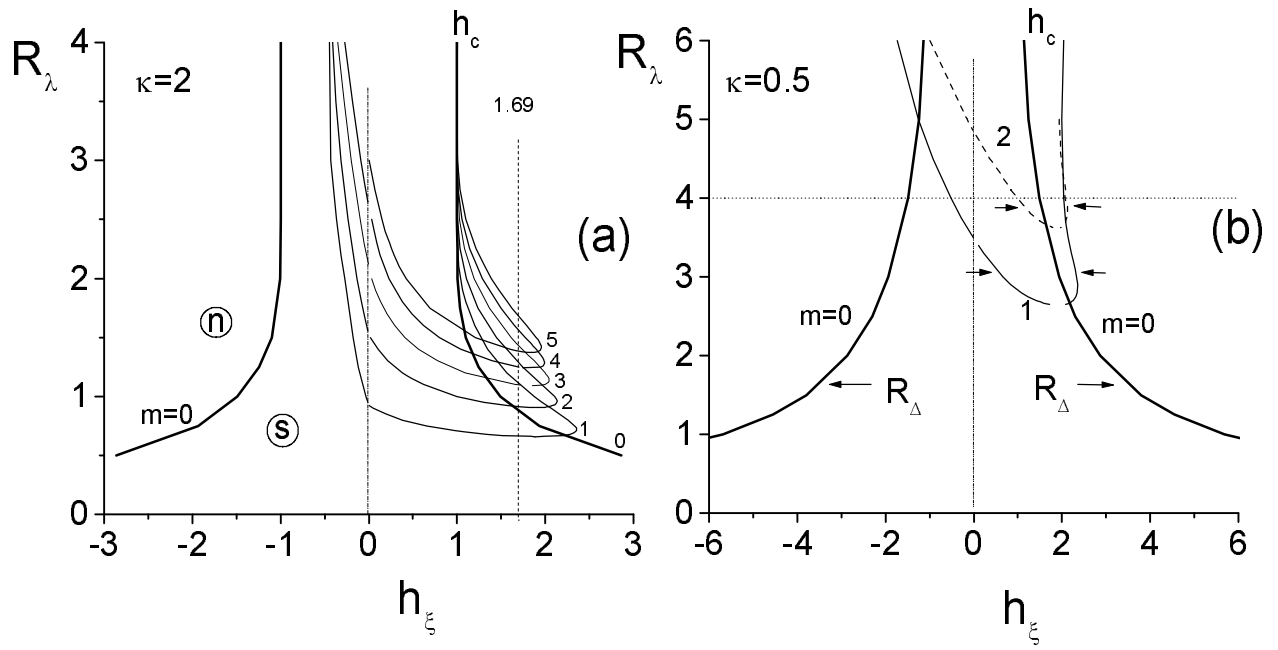


Fig.1

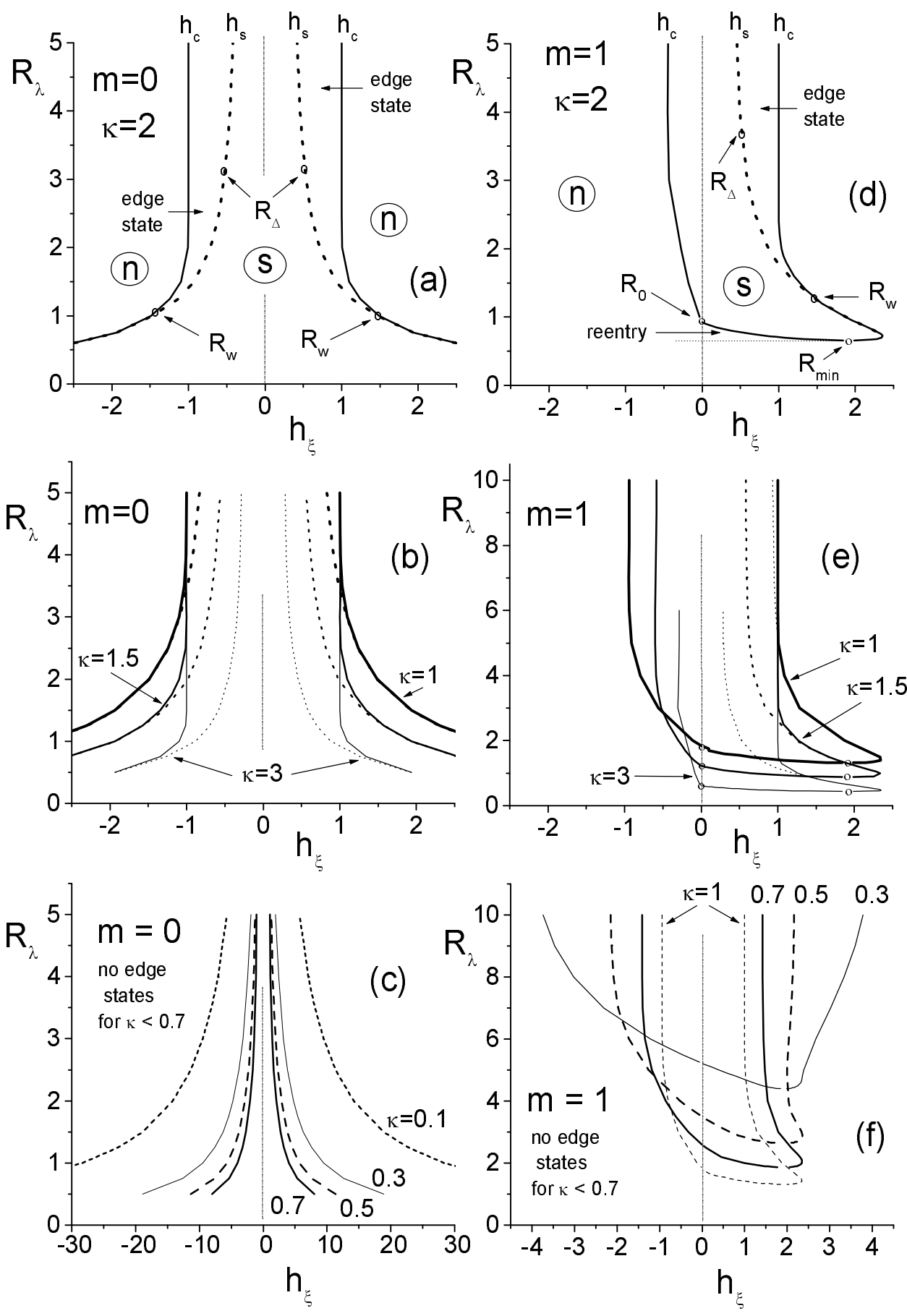


Fig.2

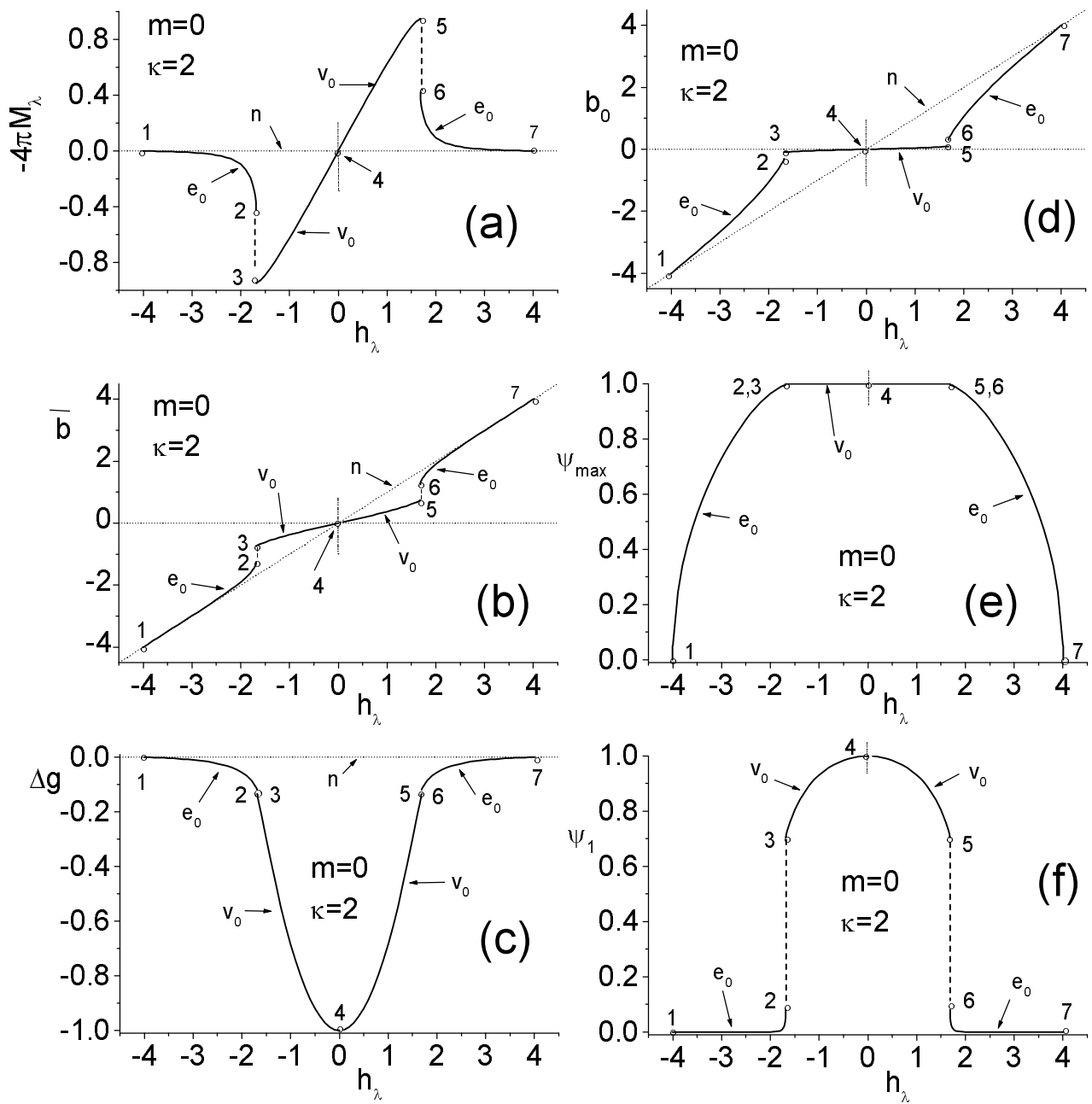


Fig.3

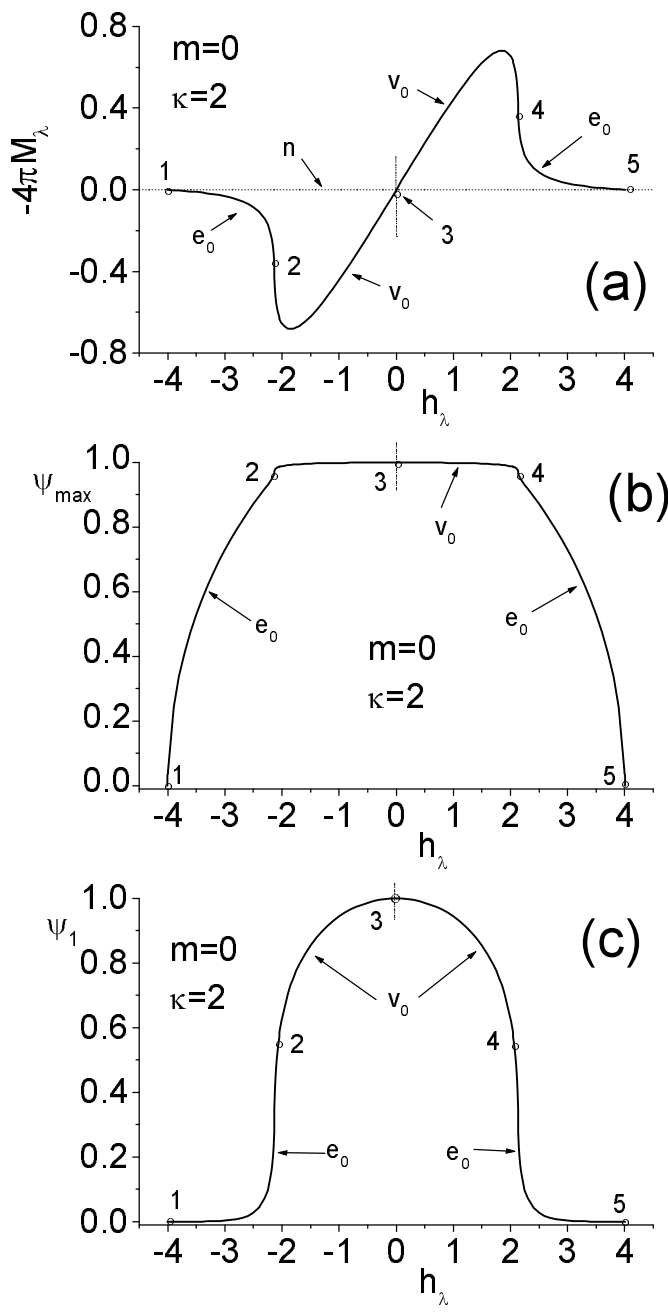


Fig. 4

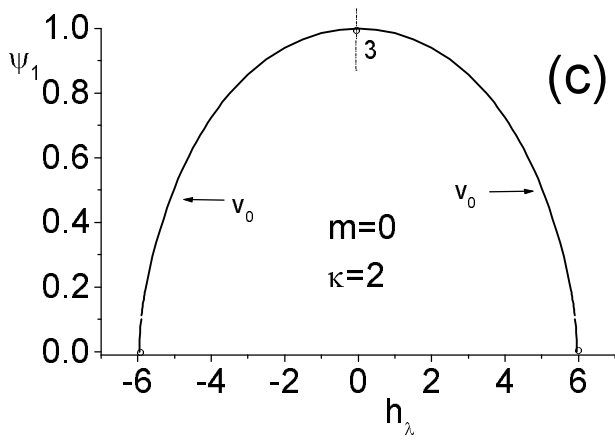
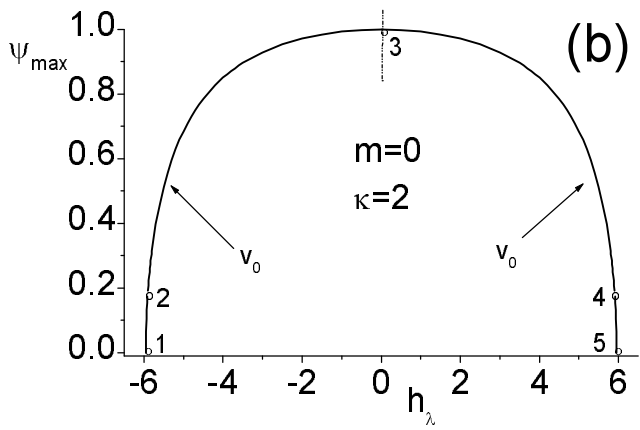
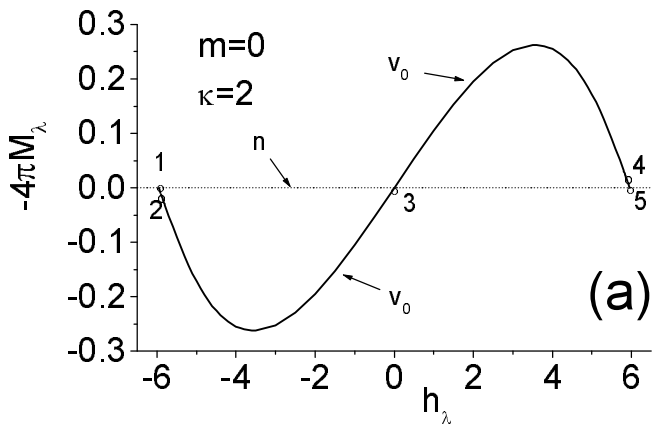


Fig. 5

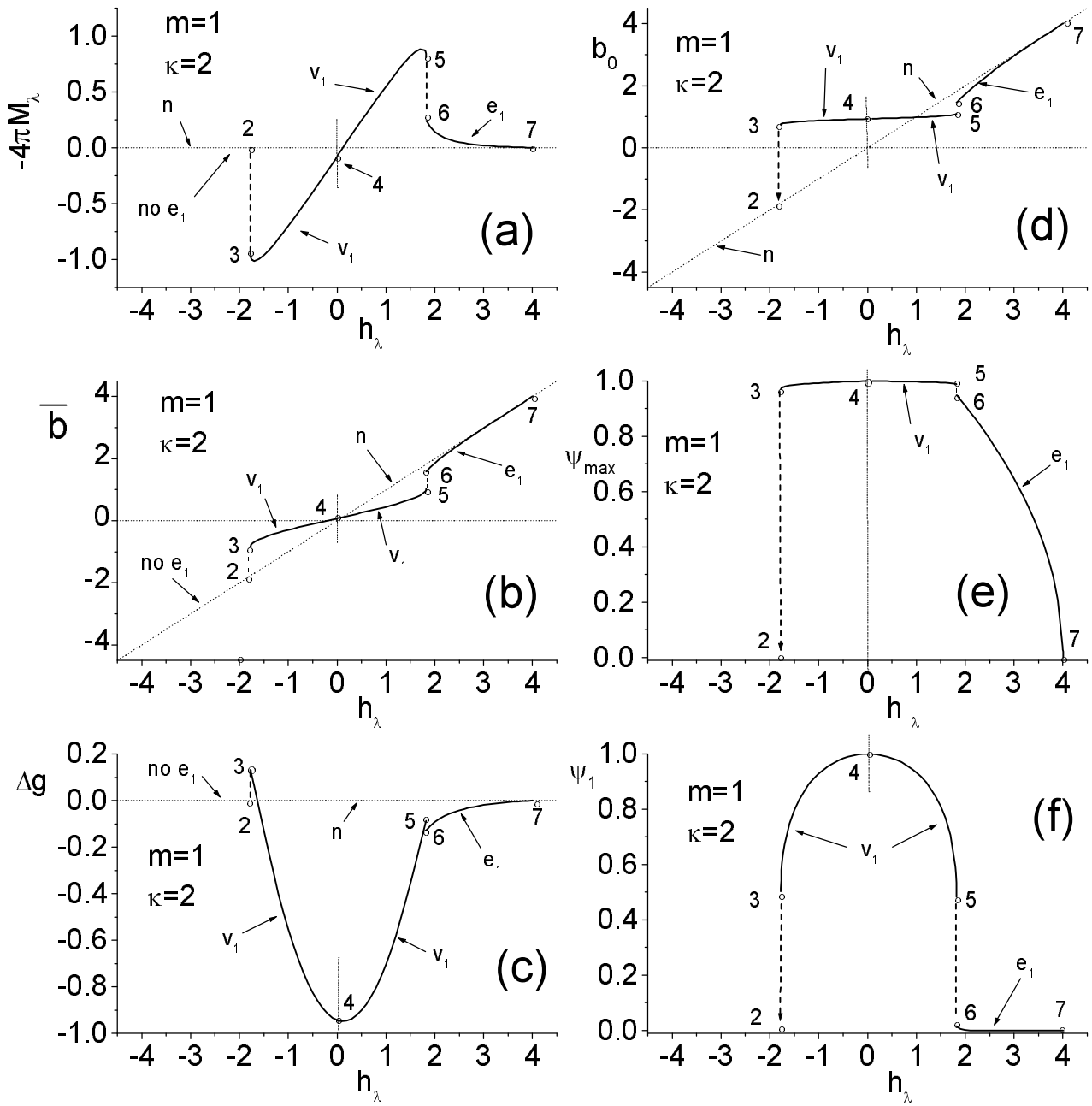


Fig. 6

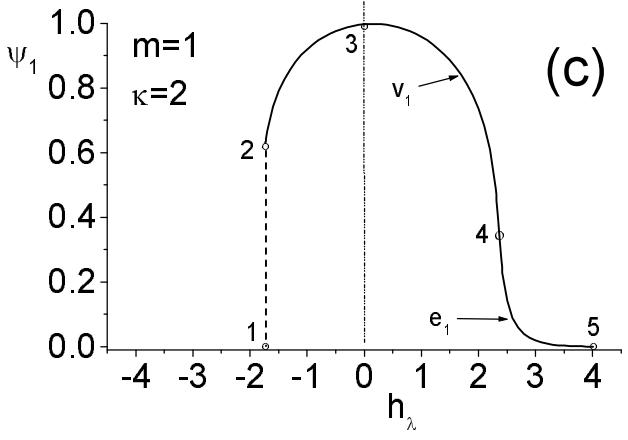
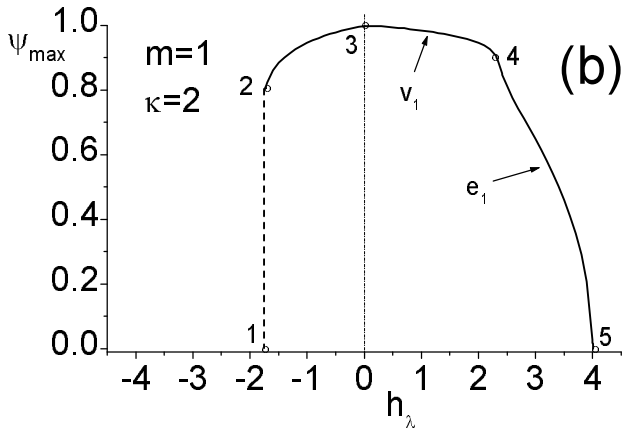
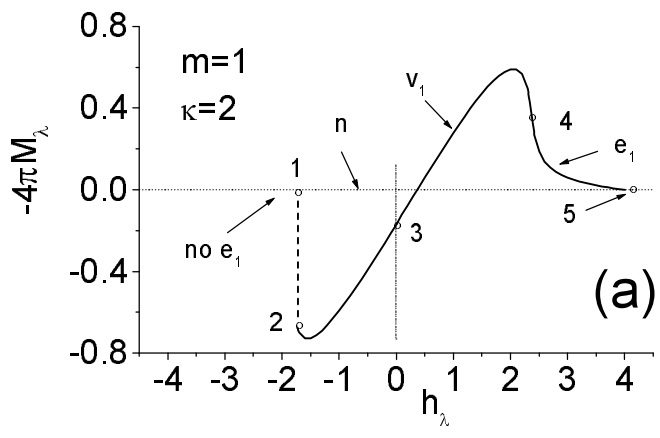


Fig. 7

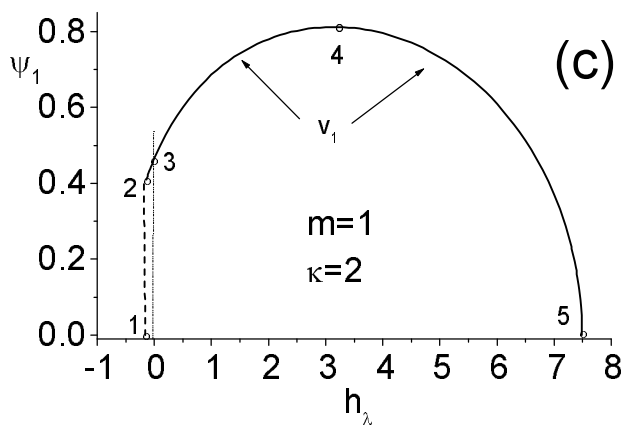
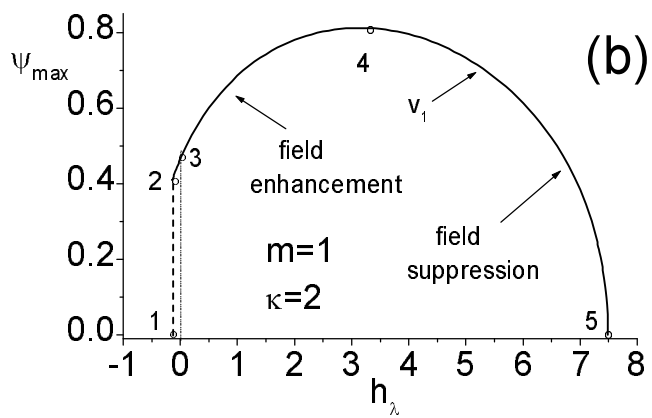
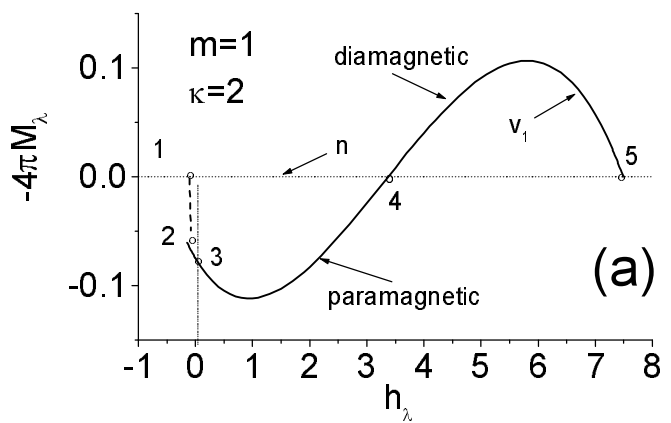


Fig. 8

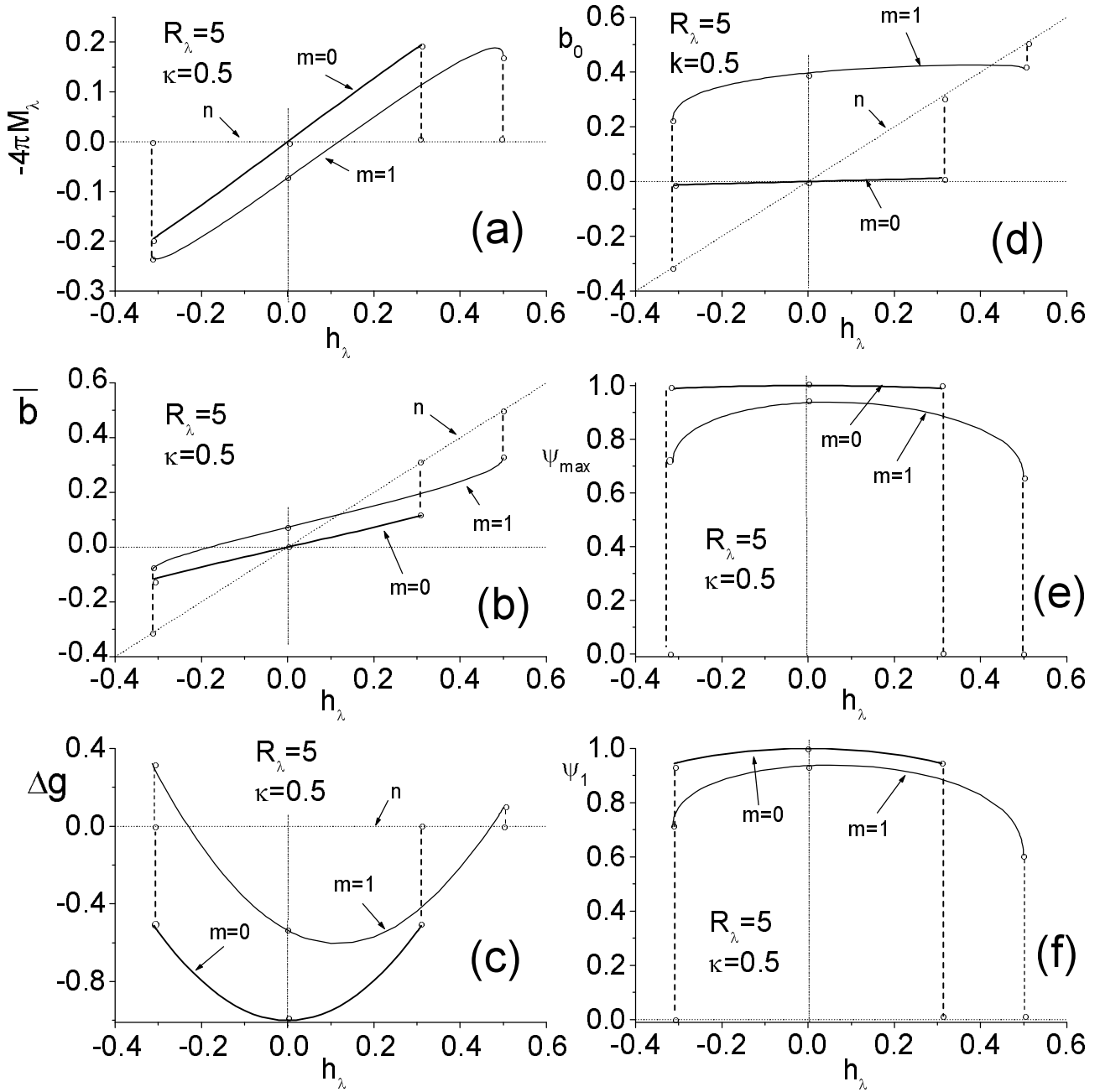


Fig.9

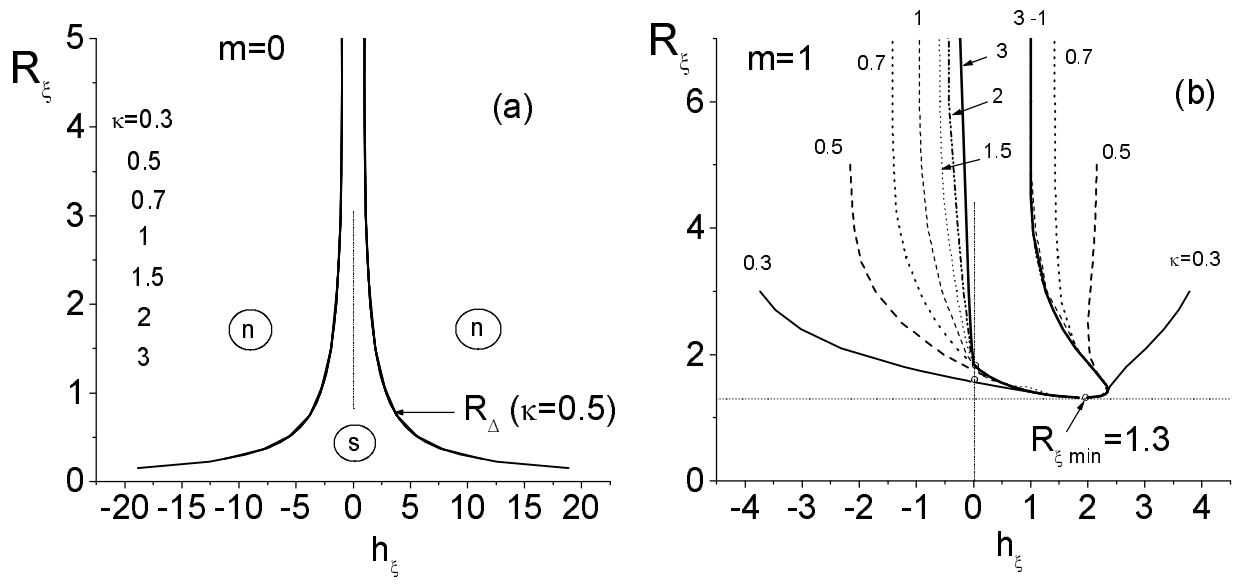


Fig.10

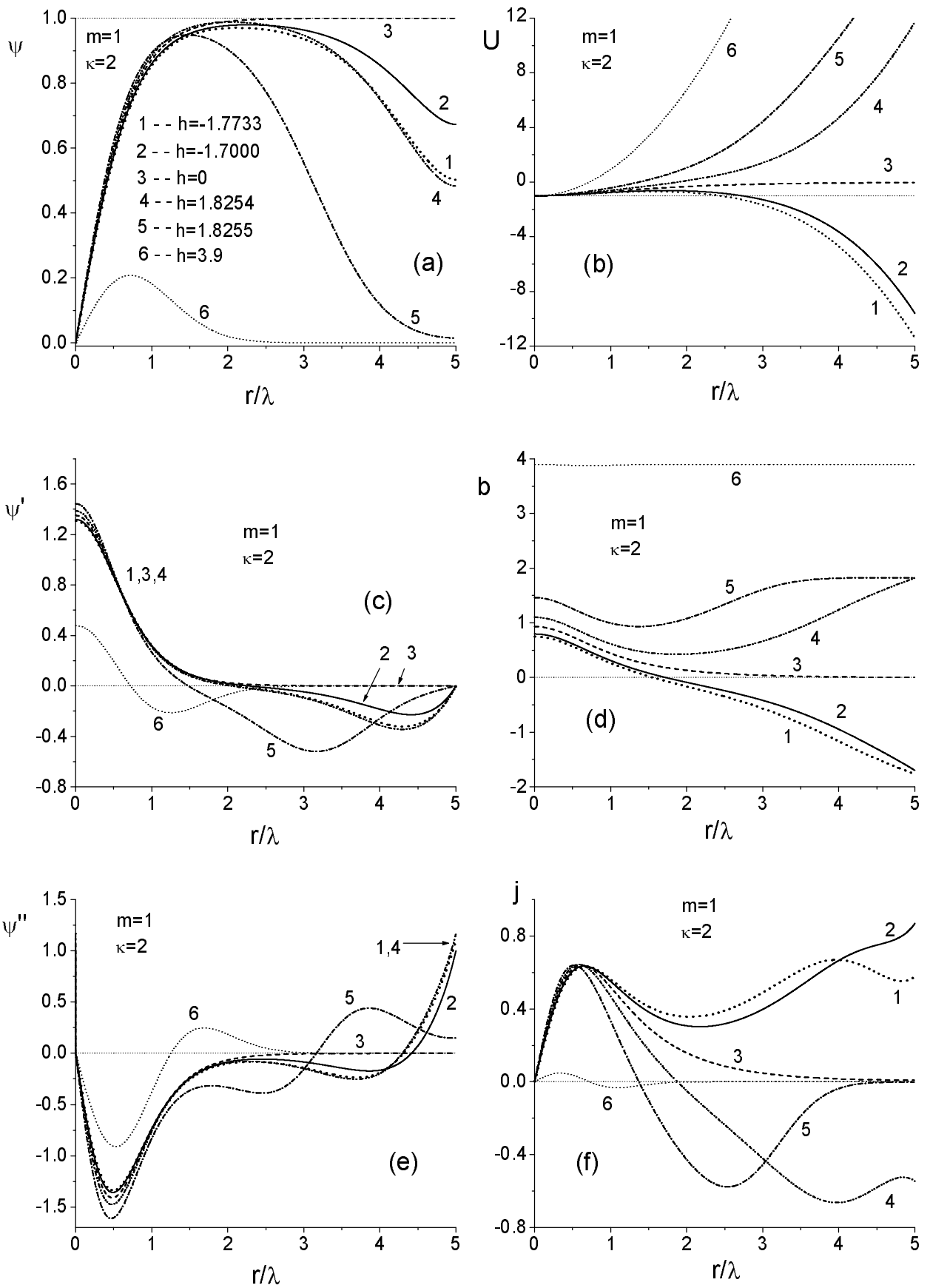


Fig. 11

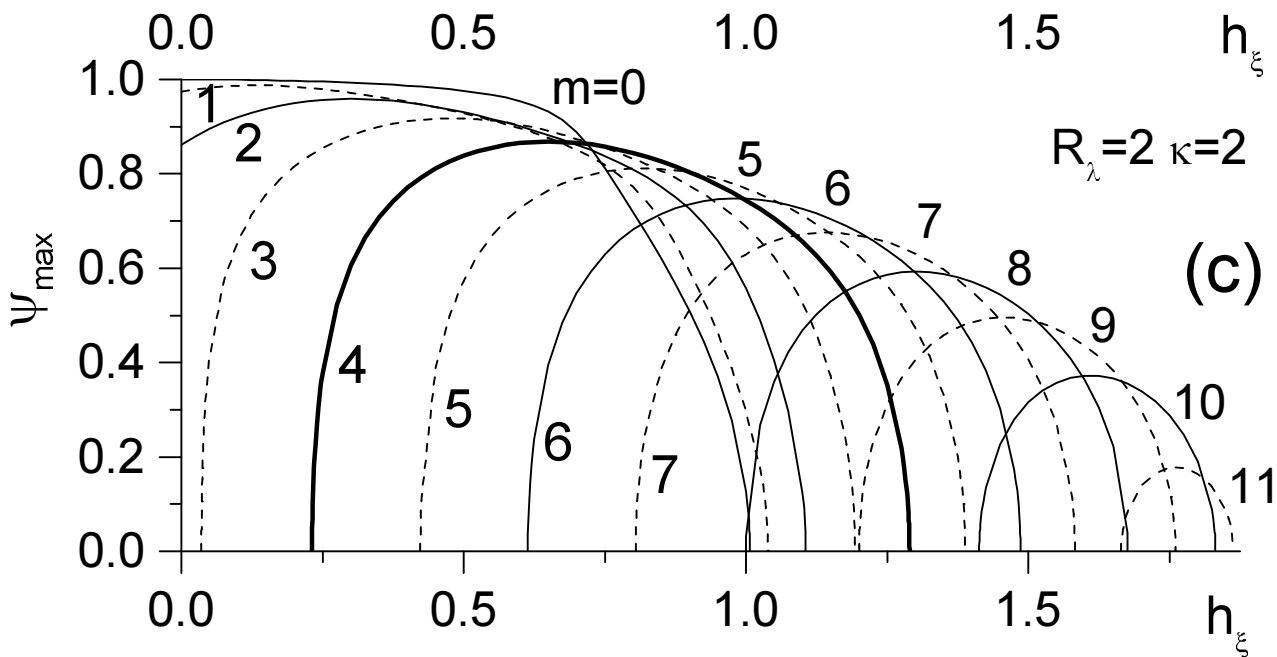
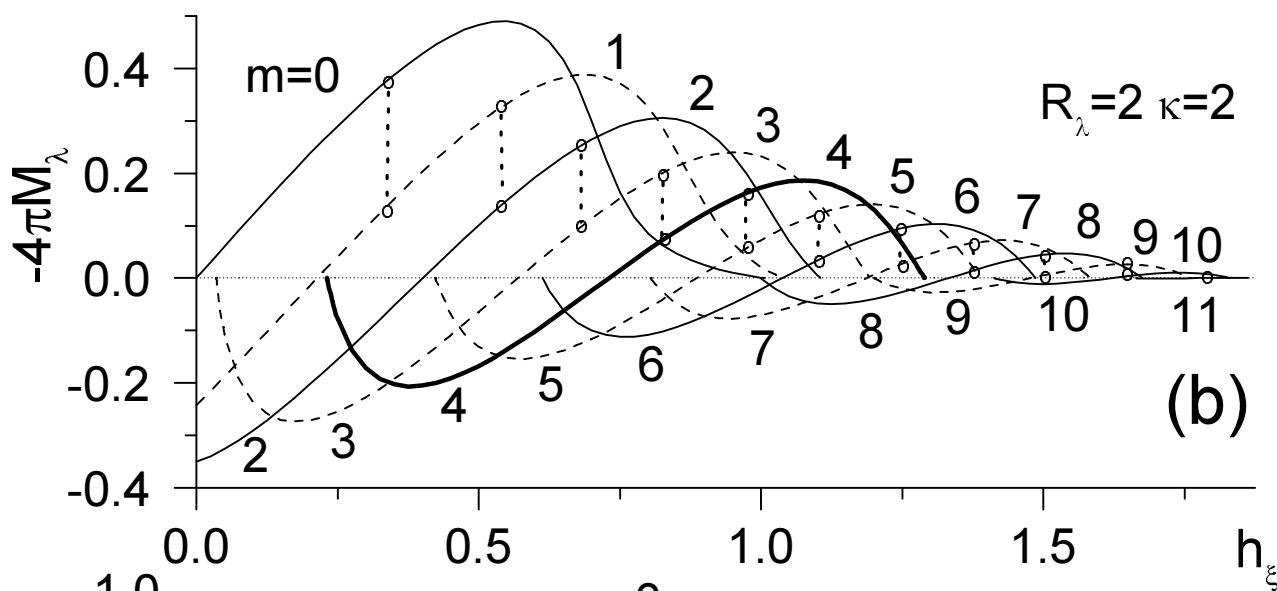
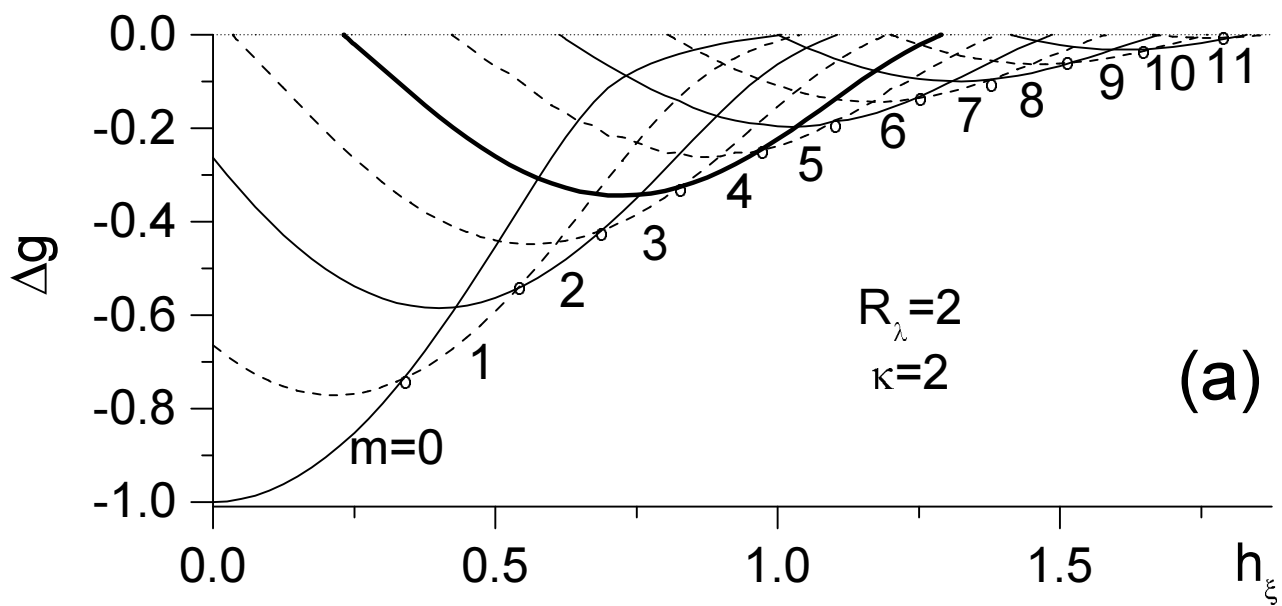


Fig. 12

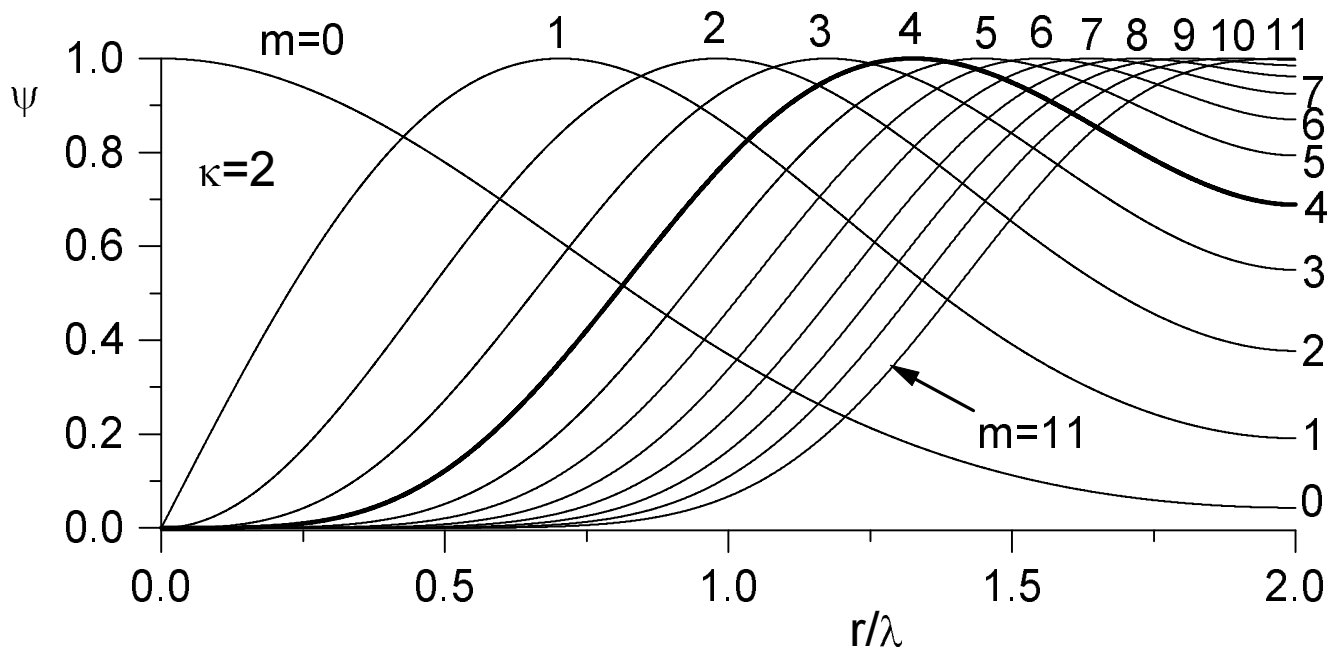


Fig. 13

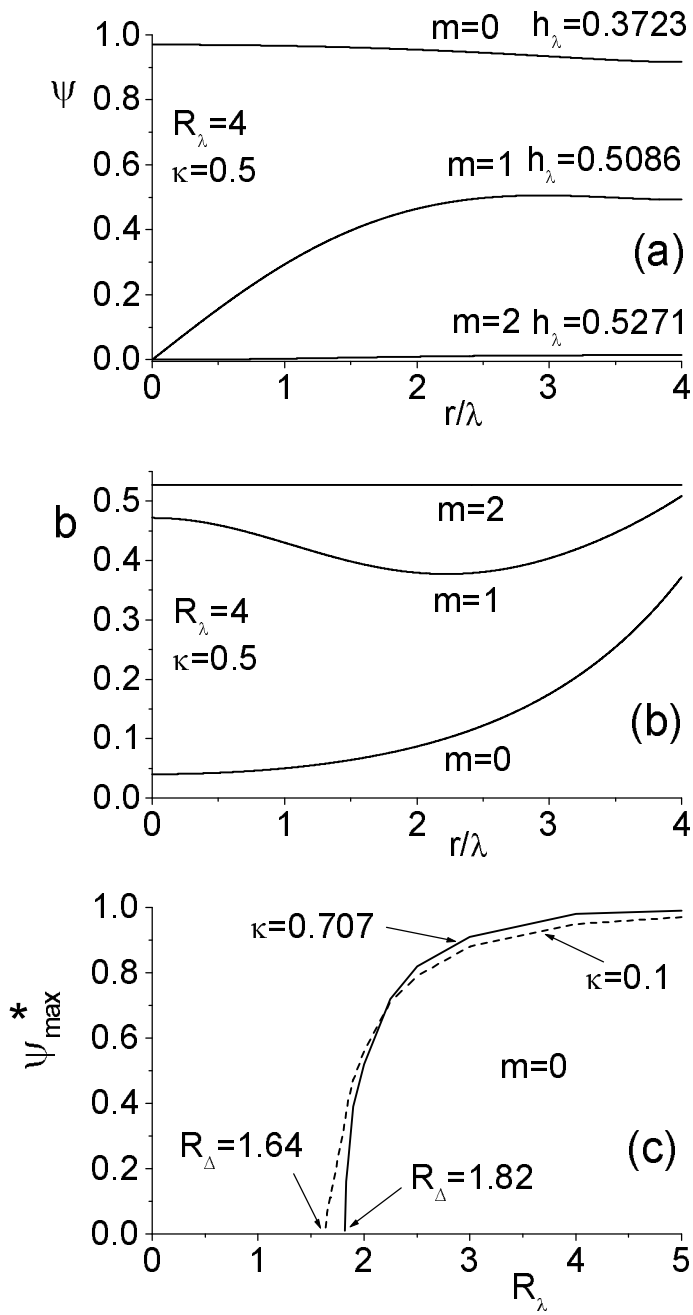


Fig. 14